



This is a repository copy of *Automatic yield-line analysis of out-of-plane loaded masonry cladding panels*.

White Rose Research Online URL for this paper:

<https://eprints.whiterose.ac.uk/219958/>

Version: Published Version

Article:

Grillanda, N., He, L. orcid.org/0000-0002-2537-2244, Gilbert, M. orcid.org/0000-0003-4633-2839 et al. (1 more author) (2024) Automatic yield-line analysis of out-of-plane loaded masonry cladding panels. *Computers & Structures*, 305. 107563. ISSN 0045-7949

<https://doi.org/10.1016/j.compstruc.2024.107563>

Reuse

This article is distributed under the terms of the Creative Commons Attribution (CC BY) licence. This licence allows you to distribute, remix, tweak, and build upon the work, even commercially, as long as you credit the authors for the original work. More information and the full terms of the licence here:

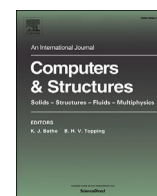
<https://creativecommons.org/licenses/>

Takedown

If you consider content in White Rose Research Online to be in breach of UK law, please notify us by emailing eprints@whiterose.ac.uk including the URL of the record and the reason for the withdrawal request.



eprints@whiterose.ac.uk
<https://eprints.whiterose.ac.uk/>



Automatic yield-line analysis of out-of-plane loaded masonry cladding panels

Nicola Grillanda^a, Linwei He^{b,*}, Matthew Gilbert^b, Colin C. Smith^b

^a Department of Architecture, University of Ferrara, Via Quartieri 8, Ferrara, 44121, Italy

^b School of Mechanical, Aerospace and Civil Engineering, University of Sheffield, Mappin Street, Sheffield, S1 3JD, UK

ARTICLE INFO

Keywords:

Yield-line analysis
Discontinuity layout optimization
Masonry panels
Out-of-plane failure

ABSTRACT

To design out-of-plane loaded masonry cladding panels, as well as modern non-loadbearing masonry panels, the yield-line method has become widely used by engineers, and features in various design codes. However, the traditional hand-based yield-line analysis method can be challenging to apply to complex or irregular shapes, since the form of the critical yield-line pattern will generally not be known in advance. The discontinuity layout optimization (DLO) procedure, previously applied to reinforced concrete slabs, is here extended to treat masonry wall panels, with (i) the flexural moment capacity modified to take account of vertical dead loads from above; and (ii) shear failure also modelled, if critical (e.g., at damp proof course level). A key benefit of DLO is that the critical yield-line pattern can be identified automatically, with a rigorous linear programming-based formulation employed to ensure that a globally optimal solution is obtained for any given numerical discretization. Given the power of modern desktop PCs, this effectively eliminates the possibility of the critical yield-line failure mechanism being missed, allowing the presented method to be applied with confidence to both regular and complex-shaped masonry panels. A range of examples are used to demonstrate the efficacy of the approach, with solutions compared with those from analytical models and experimental tests.

1. Introduction

Non-loadbearing masonry is commonly used to clad steel and concrete framed structures [1], and is also found in the gable end walls of low-rise housing developments. In contrast with historical masonry (e.g. massive ancient structures, load-bearing walls, vaulted structures, etc) where mass, interlocking and geometry have a fundamental role in collapse behaviour under horizontal actions [2–6], these masonry elements resist out-of-plane loading principally via the flexural tensile strength of the constituent masonry, with observed failure mechanisms often resembling the yield-line patterns encountered when reinforced concrete slabs are loaded to collapse [7].

For such wall panels, out-of-plane loading may stem from the presence of positive or negative (suction) wind loads, or from seismic actions. In the case of wind loads, UK design codes [8–10] and also the current Eurocode [11] have allowed the yield-line method to be applied, with the flexural tensile strength used to compute a notional plastic moment capacity at yield-lines. When modern masonry materials are employed the flexural tensile strength is relatively high, albeit the degree of ductility is low; this is in contrast to reinforced concrete slabs,

for which yield-line theory was originally conceived, where the cross-section is usually sufficiently ductile to enable formation of multiple flexural hinges. These yield at constant plastic moment capacity until the mechanism is fully developed [12]. Conversely, the post-peak behaviour of masonry is quasi-brittle in nature, with the bending moment typically decreasing relatively sharply once a crack has been initiated [13–15]. In an attempt to address this, the fracture line method was proposed by Sinha [16,17]. Nevertheless, the yield-line method has been found to predict the out-of-plane collapse behaviour of masonry panels reasonably well [18], and experimental and theoretical studies have allowed a set of typical mechanisms to be compiled for wall panels of standard geometry; see for instance the review provided in [19] and [20], with suitable analytical formulae derived in, e.g., [21,22,7]. Thus, its use remains permitted by widely used design codes such as Eurocode 6 [11]. However, in the case of irregular wall geometries, such as walls containing openings or arbitrary polygonal-shaped panels, the standard formulae are often not directly applicable and must be adapted on a case-by-case basis. This makes hand-based yield-line analysis problematic and is one of the main motivations for developing an automated yield-line analysis approach for modern non-loadbearing

* Corresponding author.

E-mail address: linwei.he@sheffield.ac.uk (L. He).

<https://doi.org/10.1016/j.compstruc.2024.107563>

Received 26 January 2024; Accepted 6 October 2024

Available online 23 October 2024

0045-7949/© 2024 The Authors. Published by Elsevier Ltd. This is an open access article under the CC BY license (<http://creativecommons.org/licenses/by/4.0/>).

masonry cladding panels, which is the main focus of the present paper. Specifically, the discontinuity layout optimization (DLO) method [23,24], described in more detail in the next section, will here be extended for this purpose.

Central to the practical application of the yield-line method to modern masonry walls is reliable evaluation of flexural tensile strength, which depends on the composition and condition of the masonry units and mortar employed [25]. Thus various analytical models, supported by experimental tests, have been proposed (e.g., [26–30]); additionally Eurocode 6 [11] provides suitable values for use in design.

The paper is organized as follows: use of the yield-line method to analyse out-of-plane failure is considered in Section 2, with the DLO procedure that automates this method described in detail. Amendments to the standard failure criteria to enable masonry cladding panels to be analysed are described in Section 3. Examples are then considered in Section 4, including layout sensitivity analyses, comparison with analytical models (the models developed by Roberts et al. [31] and Johansen [7] are used to provide reference values) and experimental results obtained by Chong [32]; also its application to more complex wall geometries is considered. Finally, conclusions and recommended future developments are presented in Section 5.

2. Automating the yield-line method of analysis

2.1. Background

Within the context of the formal theorems of plastic limit analysis, the yield-line analysis method is an upper-bound method. This means that non-conservative results will be obtained if an incorrect layout of flexural hinges, or yield-lines, is chosen. Particularly for irregular geometries, for which available data is limited, this is problematic and, since there is a danger of missing the critical mechanism when undertaking a yield-line analysis by hand, numerical models become attractive. The first numerical models conceived for masonry panels were presented in [33] and [34]. More recently, among the several numerical models presented for masonry structures [35–41], limit analysis models based on finite element discretizations and enriched with homogenization strategies have been proposed, e.g., see [42] and [43]. In particular, the use of homogenization is advantageous, since it avoids the need to model masonry units individually [44,45]. However, a precise definition of the actual yield-line pattern can require a refined discretization that can be computationally demanding. With reference to concrete slabs, the first automatic analysis procedures were proposed by Chan [46] and then by Munro and Da Fonseca [47], albeit the solutions obtained were affected by the chosen finite element mesh discretization employed. Far fewer developments have been made specifically for masonry wall panels. In recent years, an adaptive limit analysis model where the possible cracks were iteratively adjusted by means of a meta-heuristic algorithm was proposed by Chiozzi et al. [48].

A new numerical modelling strategy that, unlike previously proposed methods, produces solutions that are not significantly affected by the chosen numerical discretization was proposed in [49,24]; this approach, termed discontinuity layout optimization (DLO), discretizes a given problem using nodes that are interconnected by potential yield-lines and determines the critical ones by solving a linear programming (LP) problem. Unlike most kinematic limit analysis methods, in this case the kinematic variables are the relative displacement (or rotation) jumps along the potential lines, rather than the displacements of solid element centroids. Thus, solid elements are not defined in the initial problem discretization, but can be identified in the post-processing phase once non-zero displacement jumps corresponding to critical yield-lines have been identified. Over the years, DLO has been applied to in-plane plasticity problems [23], in-plane loaded masonry gravity wall problems [50], out-of-plane loaded concrete slab problems [24,51], as well as to simple three-dimensional problems [52].

Here a DLO-based limit analysis model is presented that extends previous work to enable the resistance of out-of-plane loaded masonry cladding panels to be computed. In previous research focused on concrete slab analysis, described in [51] and made available to practitioners in the LimitState:SLAB software [53], classical yield-line theory hypotheses were adopted; in contrast here, an enriched formulation, designed to take into account the main characteristics of masonry cladding panels, is required. Firstly, the main kinematic variables employed in the problem must now include not only normal yield-line rotations but also twisting (torsional) rotations and out-of-plane displacements. The latter allows shear failures to be represented. Even if such failures are unusual for modern masonry, unlike historical masonry in which shear and torsion require a proper representation [54,55], they can in some cases greatly affect load-bearing capacity; e.g., damp proof courses at the base of masonry walls in buildings may have reduced shear resistance; see [56]. The addition of torsional and shear degrees of freedom, in addition to normal bending rotations, leads to a *generalized* yield-line analysis formulation. Secondly, the ultimate (plastic) moments and shears need to be defined as functions of both material mechanical properties and self-weight-derived stress acting along any given potential yield-line, so as to allow the effects of compression on the lateral resistance of masonry walls to be accounted for.

2.2. Generalized yield-line analysis via discontinuity layout optimization (DLO)

A discontinuity layout optimization (DLO) formulation for the analysis of out-of-plane loaded wall cladding panels is now presented. The main steps in the DLO procedure are depicted in Fig. 1.

Considering a three-dimensional (3D) Euclidean space xyz , consider a planar domain in the xy plane representing a masonry panel, where y defines the vertical direction. The first step in the DLO formulation is to discretize the domain into N nodes, here assumed to be uniformly distributed. A layout of M potential discontinuities is defined that connects each node to every other node. A set of kinematic variables is defined by assigning three degrees of freedom to each potential discontinuity: normal rotation θ_n along the longitudinal axis of the discontinuity \mathbf{n} ; twisting rotation θ_t along the normal axis of the discontinuity \mathbf{t} ; out-of-plane displacement δ_z . These represent displacement and rotation jumps along discontinuities in an out-of-plane mechanism (see Fig. 2). Here the main kinematic variables are defined on the assumption that small displacement theory holds, such that each degree of freedom corresponds to an infinitesimal displacement (also note that, for the sake of simplicity, the kinematic variables are herein referred to as ‘displacements’ rather than ‘displacement rates’, or ‘velocities’).

With this set of kinematic variables, the kinematic limit analysis problem can be defined as follows:

$$\text{minimize} \quad \lambda \mathbf{f}_L^T \mathbf{d} = -\mathbf{f}_D^T \mathbf{d} + \mathbf{g}^T \mathbf{p} \quad (1a)$$

$$\text{subject to} \quad \mathbf{B} \mathbf{d} = \mathbf{0} \quad (1b)$$

$$\mathbf{N} \mathbf{p} - \mathbf{d} = \mathbf{0} \quad (1c)$$

$$\mathbf{f}_L^T \mathbf{d} = 1 \quad (1d)$$

$$\mathbf{p} \geq \mathbf{0} \quad (1e)$$

where λ is a load multiplier, \mathbf{f}_L and \mathbf{f}_D are respectively vectors of live and dead applied loads (where the former are loads affected by the load multiplier and the latter are permanent loads of constant magnitude), \mathbf{g} is a vector representing internal energy dissipation, \mathbf{d} contains the kinematic displacement variables, \mathbf{p} is the unknown plastic multipliers vector, and finally \mathbf{B} and \mathbf{N} are respectively the compatibility and plastic flow rule matrices.

Now Eq. (1) defines a linear programming (LP) problem, in which the objective function (Eq. (1a)) equates external and internal work. The work dissipated by external loads is computed by considering the subdomains defined by each potential yield-line, in which the subdomain

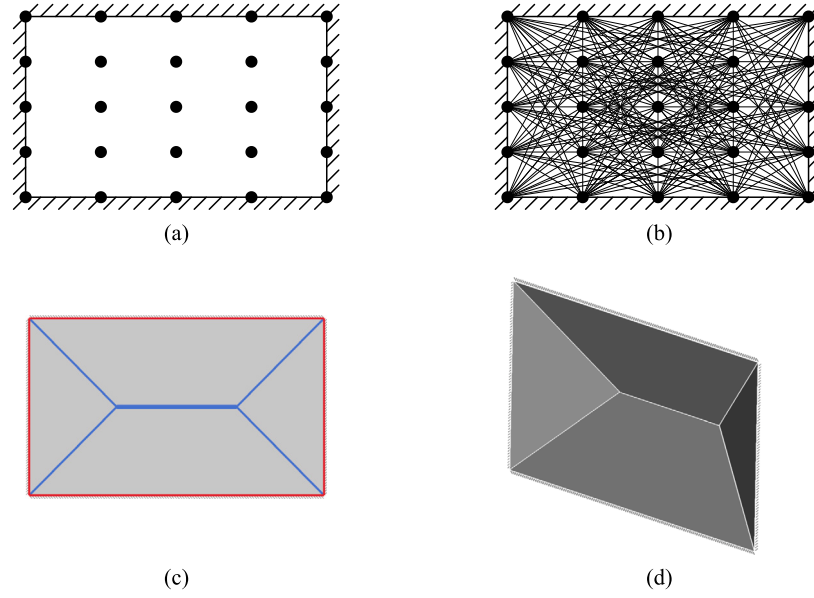


Fig. 1. Steps in the DLO analysis procedure: (a) wall area, boundary conditions and nodal discretization; (b) discontinuities (potential yield-lines) interconnecting the nodes; (c) optimized layout, defining the critical yield-line pattern; (d) associated deformed failure mechanism. (Red and blue lines represent hogging and sagging rotations respectively).

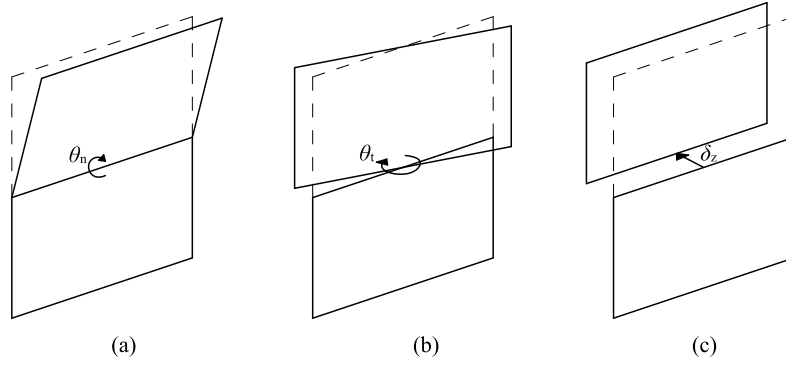


Fig. 2. Degrees of freedom for each DLO discontinuity: (a) normal rotation jump θ_n ; (b) twisting rotation jump θ_t ; (c) out-of-plane displacement jump δ_z .

is the area A_i^* of domain located above the i -th line (see Fig. 3). By considering a unit surface load W_z acting in the out-of-plane direction as a live load, the live load work for the i -th yield-line can be defined as follows:

$$\begin{aligned} \mathbf{f}_{Li}^T \mathbf{d}_i &= l_i \begin{bmatrix} m_{ni} & m_{ti} & t_i \end{bmatrix} \begin{bmatrix} \theta_{ni} \\ \theta_{ti} \\ \delta_z \end{bmatrix} \\ &= A_i^* \begin{bmatrix} W_z r_n & W_z r_t & W_z \end{bmatrix} \begin{bmatrix} \theta_{ni} \\ \theta_{ti} \\ \delta_z \end{bmatrix}, \text{ for } i = 1..M \end{aligned} \quad (2)$$

where l_i is the length of the yield-line, m_{ni} , m_{ti} and t_i denote the generalized (i.e., per unit-length) normal moment, twisting moment and out-of-plane shear contributions, r_n and r_t are the normal and longitudinal distances between the midpoint of the yield-line and the subdomain centroid (see again Fig. 3). Dead loads typically comprise wall self-weight and any compression load applied at the top edge. However, since forces and moments deriving from these actions act within the xy plane, no work is associated with the adopted kinematic variables and the associated $\mathbf{f}_D^T \mathbf{d}$ quantity is zero.

Before considering the internal work, equality and inequality constraints are described. Thus the kinematic admissibility for the displacements field is imposed through Eq. (1b), in which the \mathbf{B} matrix is built by assembling the compatibility constraints defined for each yield-line:

$$\mathbf{B}_i \mathbf{d}_i = \begin{bmatrix} \alpha_i & -\beta_i & 0 \\ \beta_i & \alpha_i & 0 \\ 0 & \frac{l_i}{2} & 1 \\ -\alpha_i & \beta_i & 0 \\ -\beta_i & -\alpha_i & 0 \\ 0 & \frac{l_i}{2} & -1 \end{bmatrix} \begin{bmatrix} \theta_{ni} \\ \theta_{ti} \\ \delta_{zi} \end{bmatrix} = \mathbf{0}, \text{ for } i = 1..M \quad (3)$$

where α_i and β_i represent respectively the cosine and sine of the inclination angle of the i -th yield-line. Note that, in general, the right-hand term in Eq. (1b) represents nodal displacement jumps of the external reference system, which are zero in the absence of *a priori* imposed displacements. This indicates that the overall size of \mathbf{B} is $3N \times 3M$. Eq. (1c) represents flow rule constraints, written as follows for each potential yield-line:

$$\mathbf{N}_i \mathbf{p}_i - \mathbf{d}_i = \begin{bmatrix} 1 & -1 & 0 & 0 & 0 & 0 \\ 0 & 0 & 1 & -1 & 0 & 0 \\ 0 & 0 & 0 & 0 & 1 & -1 \end{bmatrix} \begin{bmatrix} p_i^1 \\ p_i^2 \\ p_i^3 \\ p_i^4 \\ p_i^5 \\ p_i^6 \end{bmatrix} - \begin{bmatrix} \theta_{ni} \\ \theta_{ti} \\ \delta_{zi} \end{bmatrix} = \mathbf{0},$$

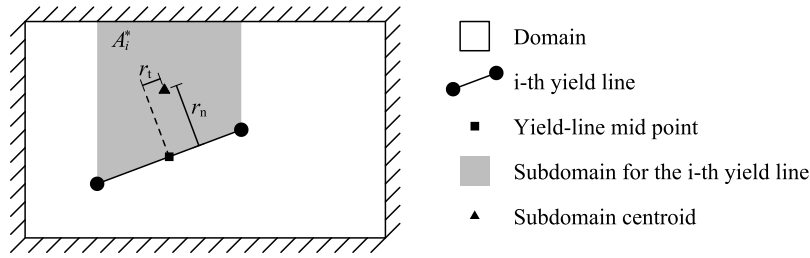
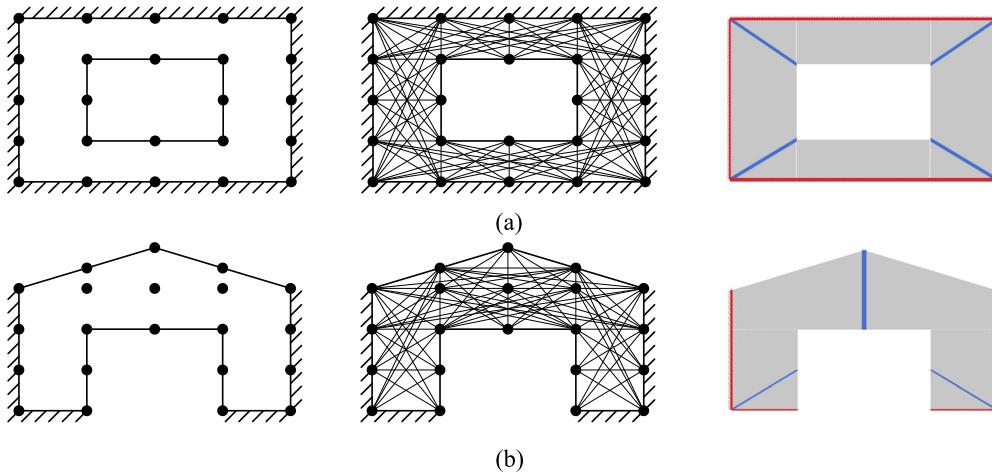
Fig. 3. Geometrical quantities characterizing the subdomain of the i -th yield-line.

Fig. 4. Using DLO to handle problems involving: (a) a wall with an opening; (b) a more complex wall geometry.

$$\text{for } i = 1 \dots M \quad (4)$$

that results in an overall \mathbf{N} matrix of size $3M \times 6M$. The six plastic multipliers \mathbf{p}_i derive from the assumed yield function f :

$$f(m_n, m_t, t) = \begin{cases} |m_{ni}| \leq m_{pni} \\ |m_{ti}| \leq m_{pti} \\ |t_i| \leq t_{pi} \end{cases}, \text{ for } i = 1 \dots M \quad (5)$$

where m_{pni} , m_{pti} and t_{pi} are the generalized plastic normal moment, twisting moment and out-of-plane shear for the i -th yield-line. In contrast to the DLO formulation proposed for concrete slabs [24], here the quantities defining the yield function are expressed as a function of the mechanical properties of the masonry and the vertical loads acting on the yield-line, described in more detail in Section 3. The definition of the internal plastic dissipation vector \mathbf{g}_i for the i -th yield-line stems directly from Eq. (5):

$$\mathbf{g}_i^T = [m_{pni} \ m_{pti} \ m_{pti} \ m_{pti} \ t_{pi} \ t_{pi}] l_i, \text{ for } i = 1 \dots M \quad (6)$$

Finally, Eqs. (1d) and (1e) respectively normalize the live load work and ensure that the plastic multiplier variables are non-negative. According to classical yield-line theory [57], torsional and out-of-plane shear displacements are assumed to be zero. Thus the formulation presented here could be simplified to represent the classical yield-line analysis formulation by limiting the degrees of freedom to the normal rotations θ_n and removing the other kinematic variables together with the associated plastic multipliers for each internal line (as shown in [51]). Note that for boundary lines twisting rotations θ_t and out-of-plane displacements δ_z are not zero for some boundary conditions, e.g., cases involving free boundaries or lines of symmetry (where for the latter only δ_z is non-zero); thus these variables must be maintained for such lines even within the classic formulation. However, in the presented approach twisting rotations and out-of-plane displacements are also maintained

for internal yield-lines to allow for possible torsional and shear failures; this gives rise to a generalized limit analysis formulation for out-of-plane loaded masonry panels.

Solving Eq. (1) furnishes a load multiplier and set of displacement and rotation jumps that identify active yield-lines in the mechanism. By definition, the obtained load multiplier is a kinematic multiplier, thus defining an upper bound on the collapse load, which becomes closer and closer to the true collapse multiplier as the numerical discretization is refined (i.e., the number of nodes is increased). This is reflected in the geometrical representation of the collapse mechanism, which depends on the density of the nodal grid employed and the associated layout of potential yield-lines.

Finally, it is worth noting that the presented DLO procedure can be readily applied to complex geometries, involving openings and/or non-convex polygonal shapes [24]. In these cases, an initial layout defined on the domain convex-hull is adjusted by removing any nodes and potential yield-lines lying outside the real domain, or inside any openings; see Fig. 4.

3. Applicable masonry properties

Fundamental properties associated with out-of-plane failure of a wall panel formed from modern masonry are now presented. As noted previously, the adopted formulation generalizes classical yield-line theory, in which mechanisms are assumed to involve flexural hinges only. Thus, although failures involving out-of-plane bending are most common, the potential for out-of-plane shear/torsion failure should not be discounted and therefore both are considered herein.

3.1. Out-of-plane bending failure

Differently from the previous application to reinforced concrete slabs [24], for masonry cladding panels the generalized plastic bending mo-

ments must take into account the contribution of self-weight (and any other vertical load if present). Moreover, for a heterogeneous material like masonry, the orthotropic behaviour corresponding to the actual texture should be considered. Therefore, separate plastic moment capacities are defined for bending in the x and y directions. Considering a stretcher (or ‘running bond’) masonry texture, and by maintaining the external reference configuration introduced in Section 2.2, x and y respectively correspond to directions parallel and orthogonal to bed joints. The generalized plastic bending moments can be defined as follows:

$$m_{px} = \frac{(f_x + \sigma_y)t^2}{6} \quad (7a)$$

$$m_{py} = \frac{f_y t^2}{6} \quad (7b)$$

where f_x and f_y are the flexural tensile strengths on the xz and yz planes respectively, σ_y is the compression stress deriving from the vertical load (i.e., due to wall self-weight and compression loads at the top of the wall), and t is the wall thickness. It can be observed that the generalized bending moment capacity m_{px} will take on different values for each yield-line. Specifically, this depends on the vertical stress value, which can be evaluated as follows:

$$\sigma_y = \gamma(h - y) + \frac{q_y}{t} \quad (8)$$

where γ is the weight per unit volume of masonry, q_y is the magnitude of any vertical load applied at the top of the wall panel (assumed positive if it is compressive), h is the height of the wall and y denotes the point at which the vertical stress is evaluated (generally the midpoint of the line). Note that the quantity q_y is typically null for cladding panels, thus the self-weight is the only vertical load affecting the generalized plastic bending moment m_{px} . According to the adopted reference system, f_x represents the flexural strength of a horizontal mortar bed joint, whereas f_y represents the flexural strength of the masonry about a vertical axis. Estimated values for f_y can be obtained from Eurocode 6 [11] (in turn derived from [31]) for different mortar and brick unit properties. In some cases, these data are provided in terms of orthogonal ratios $\mu = f_{kx}/f_{ky}$, where f_{kx} and f_{ky} are the characteristic flexural tensile strength values for the two main directions.

Alternatively, a suitable analytical model for stretcher / running bond masonry textures was proposed in [27], in which the following equation for m_{py} is suggested:

$$m_{py} = \min \left\{ \frac{l_u + t_j}{2(h_u + t_j)} \tau_x k_b t^2; \frac{f_{ut} - \nu \sigma_y}{2} \frac{t^2}{6} \right\} \quad (9)$$

where l_u and h_u are respectively the length and height of the masonry unit, t_j is the thickness of the mortar joint, τ_x is the tangential stress acting on the bed joint, k_b is a numerical factor that depends on the geometry of the bed joint (after [58]), f_{ut} is the flexural tensile strength of the masonry unit, and finally ν is the Poisson's ratio of the masonry. According to Eq. (9), the horizontal bending strength for a vertical yield-line arises due to torsional failure of bed joints or bending failure of brick units. In fact, Eq. (9) is likely to provide a conservative strength estimate since it prescribes that the bending strength is the minimum of the resistances associated with these two failure modes, with any contribution provided, e.g., by vertical mortar joints being neglected. By using Eq. (9) and by assuming $\tau_x = 1.6f_x + 0.9\sigma_y$, again as suggested by [27], an equivalent value for f_y can be derived:

$$f_y = \min \left\{ \frac{3(l_u + t_j)}{h_u + t_j} (1.6f_x + 0.9\sigma_y) k_b; \frac{f_{ut} - \nu \sigma_y}{2} \right\} \quad (10)$$

By following this model, m_{py} also becomes dependent on the vertical stress σ_y . Whatever values are assumed for the main generalized plastic bending moment capacities, the moment capacity m_{pni} for any inclined

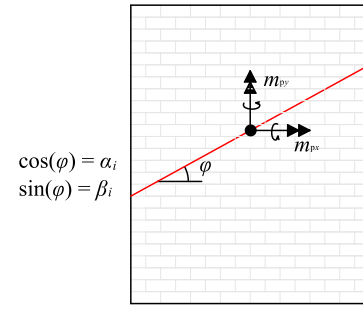


Fig. 5. Plastic bending moments for an inclined yield-line in a masonry wall panel.

yield-line (with corresponding cosine α_i and sine β_i - see Fig. 5) can be obtained by following the formula suggested in [7]:

$$m_{pni} = m_{px} \alpha_i^2 + m_{py} \beta_i^2 \quad (11)$$

It can be observed that the bending moment capacity of an inclined yield-line does not directly take into account the actual masonry texture. This can be addressed by following a homogenization procedure, in which any inclined bending moment also depends on the size and arrangement of units. Homogenization would allow to fully extend DLO to historical structures, as well as load-bearing masonry structures, in which the structural behaviour is highly affected by interlocking and overall geometry (see [59]); this is the subject of future work.

Note that the presented bending moment equations can be used for single-leaf panels. For double-leaf walls with free sliding between the two leaves, or masonry composed of hollow blocks, the generalized plastic bending moments must be adapted; e.g., the following formulae can be used for m_{px} in the case of double-leaf walls and hollow block masonry:

$$m_{px} = \frac{f_x + \sigma_y}{6} \cdot \frac{t_1^3 + t_{II}^3}{\max\{t_1, t_{II}\}} \quad (12a)$$

$$m_{px} = \frac{(f_x + \sigma_y)(1 - e^2)t^2}{4} \quad (12b)$$

where t_I and t_{II} are the thickness values of the two leaves, and e ($0 \leq e < 1$) is a parameter defining the dimension of the cavity within hollow blocks (see Fig. 6).

3.2. Out-of-plane shear failure

When considering out-of-plane shear failure, both plastic shear forces and twisting moments need to be accounted for, expressed with reference to the shear strength f_v as follows:

$$t_p = f_v t \quad (13)$$

and

$$m_{pti} = \frac{f_v t l_i}{6} \quad (14)$$

Note that the generalized twisting moment depends on the length l_i of the yield-line on which it is computed. Eq. (14) was derived by assuming a linearly varying transverse shear stress having maximum value f_v at the extremities of the line. This assumption follows the standard shear design of concrete slabs, in agreement with [60] and [61]. By considering a linear shear stress distribution reaching the shear strength f_v at extremities only, Eq. (14) represents a crack initiation twisting moment and, according to [61], can be used as a safe design limit for the twisting moment. In absence of specific details from Eurocode for out-of-plane twisting failures in modern masonry panels, the assumptions recommended for concrete slabs have been followed here, incorporating a shear strength expression suitable for modern masonry. Note also

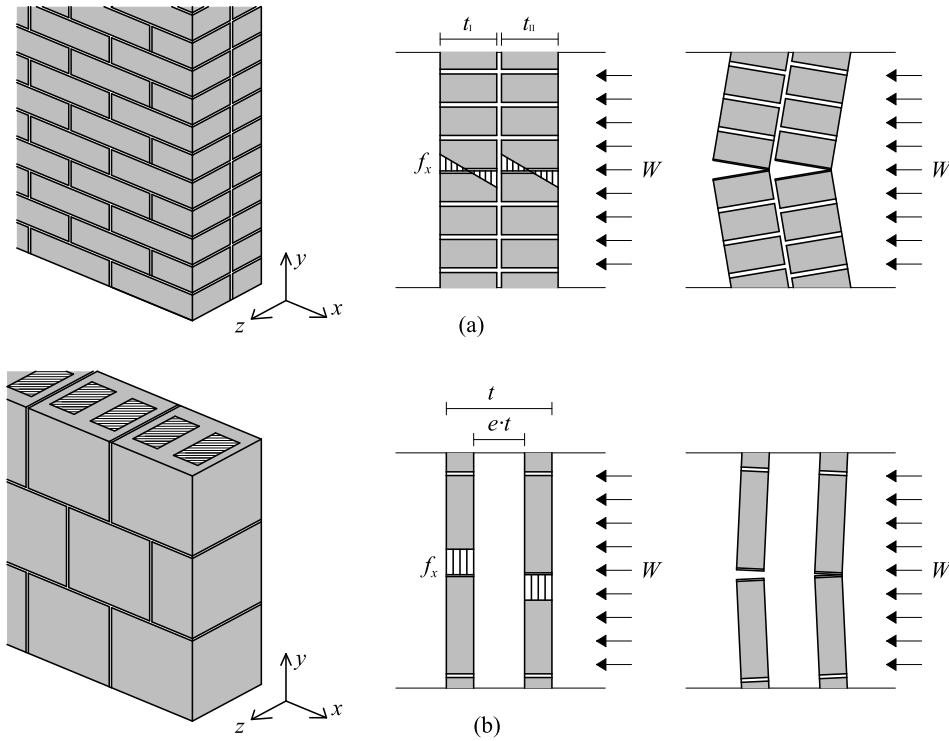


Fig. 6. Representation of plastic bending moments and expected flexural hinges: (a) double-leaf (free sliding between the two leaves); (b) hollow block masonry.

Boundary condition	Symbol	Internal dissipation vector
Fixed		$\mathbf{g}_i^T = [m_{pn}, m_{pt}, t_p] l_i$
Partially fixed		$\mathbf{g}_i^T = [\phi m_{pn}, m_{pt}, t_p] l_i, 0 < \phi < 1$
Supported		$\mathbf{g}_i^T = [0, m_{pt}, t_p] l_i$
Symmetry		$\mathbf{g}_i^T = [m_{pn}, 0, 0] l_i$

Fig. 7. Boundary conditions: graphical representation and corresponding internal dissipation.

that, differently from [54], the generalized bending and twisting moment remain uncoupled. This is accepted for modern non-loadbearing masonry panels where shear effects are rarely observed. For historical and load-bearing masonry structures, the coupling between bending, torsion and shear effects could be achieved, for example, through homogenization techniques [59] (as previously mentioned, such topic will be investigated in a future work more focused on historical masonry).

The shear strength along bed joints is prescribed in Eurocode 6 [11] (again derived from [31]):

$$f_v = \min\{f_{v0} + 0.4\sigma_y; 0.065f_c\} \quad (15)$$

where f_{v0} is the shear strength under zero compression stress, 0.4 is the assumed coefficient of friction, and f_c is the compression strength. The obtained value can be reduced in certain situations, for instance in the presence of unfilled vertical joints (refer to [11] for more details). In particular, in the presence of a damp proof course (DPC) the actual shear strength can be much lower than the results indicated by Eq. (15); see [56]. The exact value depends on the type of damp-proof course adopted but, according to Roberts et al. [31], damp-proof course mortar joints should provide a minimum shear strength of 0.09 MPa. As regards to computation of the shear strength orthogonal to bed joints, the Eurocode

does not provide specific information, though in [31] a value of $2f_v$ is recommended.

4. Numerical examples

The presented DLO analysis formulation is now applied to various out-of-plane loaded masonry panel examples. Firstly, the sensitivity of the collapse load to the initial layout is investigated by using two simple examples. Secondly, results are compared with those from analytical models developed by Roberts et al. [31] and Johansen [7]. Using problems with both simple and slightly more complex geometrical configurations, the results are also compared with those from Eurocode 6 [11], in this case with partial safety factors included in the calculations. Thirdly, DLO results are compared with experimental data presented by Chong [32]. Finally, various more challenging examples are considered, involving gable wall geometries involving complex polygonal shapes and openings, typical of those found in UK buildings; these are included to more fully demonstrate the potential of the presented method. For sake of clarity, the values of all key geometrical parameters (height h , length L and thickness t of the panel; also breadth a and height b of an opening, if present) and mechanical parameters (resistance values and partial safety factors) adopted in the examples presented are reported

Table 1
Geometrical and material parameters used in the numerical examples.

Wall example:	Simply supported panel	Fixed panel	Panel with weak base shear joint	Fixed panel with opening	Chong's walls	Gable walls
Section:	4.1 & 4.2.1	4.1	4.2.2	4.2.3	4.3	4.4
Geometry [m]	$h = L = 3$ & $0.4 \leq \frac{h}{L} \leq 1.6$, $h = 3$	$h = L = 3$	$0.4 \leq \frac{h}{L} \leq 1.6$, $h = 3$	$h = L = 4$, $0 \leq \frac{a}{L} \leq \frac{1}{2}$, $0 \leq \frac{b}{h} \leq \frac{1}{2}$	Fig. 21	Fig. 23
Thickness t [mm]	102.5 & 215	102.5	215	102.5	102.5	102.5 & 215 [Fig. 23a-d & e]
Unit weight [kN/m ³]	19	19	19	19	18	19
Characteristic horizontal flexural strength f_{kx} [MPa]	0.25	0.25	0.25	0.25	-	0.25
Orthogonal ratio $\mu = f_{kx}/f_{ky}$	0.56	0.56	0.56	0.42	-	0.56
Shear strength under zero compression stress f_{v0} [MPa]	0.35	0.35	0.35	0.35	0.35	0.35
Material partial safety factor λ_m	3.1	3.1	3.1	3.5	-	3.1
Material partial safety factor in shear λ_{mv}	2.5	2.5	2.5	2.5	2.5	2.5
Partial safety factor on the loading λ_f	1.2	1.2	1.2	1.2	-	1.2
Horizontal flexural strength f_x [MPa]	$\frac{f_{kx}}{\lambda_m}$	$\frac{f_{kx}}{\lambda_m}$	$\frac{f_{kx}}{\lambda_m}$	$\frac{f_{kx}}{\lambda_m}$	0.74	$\frac{f_{kx}}{\lambda_m}$
Vertical flexural strength f_y [MPa]	$\frac{f_{ky}}{\lambda_m}$	$\frac{f_{ky}}{\lambda_m}$	$\frac{f_{ky}}{\lambda_m}$	$\frac{f_{ky}}{\lambda_m}$	2.09	$\frac{f_{ky}}{\lambda_m}$
Shear strength f_v [MPa]	Eq. (15)	Eq. (15)	Eq. (15), 0.01 at the base	Eq. (15)	Eq. (15)	Eq. (15)
Compression strength f_c [MPa]	3.5	3.5	3.5	7	3.5	3.5

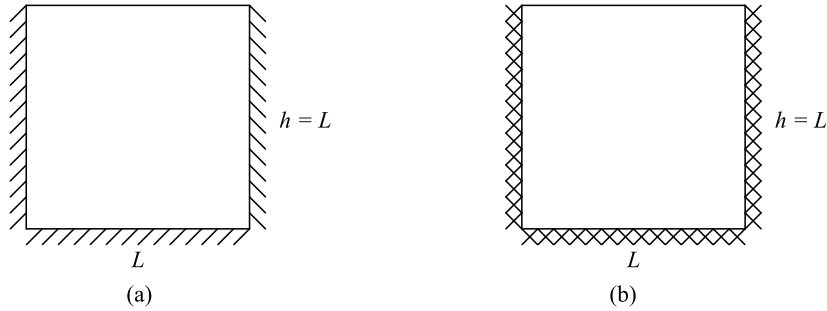


Fig. 8. Examples adopted to investigate the sensitivity of the collapse load to node distribution: (a) simply supported panel; (b) fixed panel. Geometries and boundary conditions.

in Table 1. Note that for the examples considered herein, the internal dissipation vector \mathbf{g} (Eq. (6)) varies according to the nature of the external boundaries involved; see Fig. 7. Finally, a modified version of the LimitState:SLAB [53] analysis software is used to perform the DLO calculations.

4.1. Sensitivity to node distribution

Two square panels are used to study the sensitivity of the collapse load to the node distribution. The first case is simply supported along three edges, and the second case is fixed supported, see Fig. 8. The nodal grids are equally spaced using a nodal spacing value, here indicated as $step$. In addition to evenly distributed nodal grids, a special case is considered, where the boundary lines are discretized with more nodes using a smaller nodal step: $step_{edge} \leq step_{internal}$, where $step_{edge}$ is the nodal spacing along boundary lines, and $step_{internal}$ is that for internal nodes within the domain.

Results are presented in Figs. 9 and 10. It can be seen that they converge very rapidly to asymptotic value. Relatively accurate (0.03% and 0.43% difference for supported and fixed panel respectively) collapse loads are obtained with 44 nodes per m² (corresponding to $step_{internal} = 0.15$ m). In Fig. 9, refining the boundary line (i.e., using a lower nodal spacing along edges) has negligible influence on the obtained result, since the mechanism is mainly governed by the internal yield-lines. A different situation is observed in Fig. 10, where the additional yield-lines close to the corners result in more accurate solutions. Nevertheless,

the differences become negligible when a fine nodal grid is employed. In all the following examples, approximately 220 nodes per m² (corresponding to an internal nodal spacing equal to 0.067 m) are used.

4.2. Comparison with traditional analytical models

4.2.1. Simply supported panel

The first example is a simple rectangular wall panel. As shown in Fig. 11a, the wall is modelled as a single-leaf panel simply supported on three edges, with a free top edge. Differently from the example in the previous subsection, here different h/L aspect ratios are considered. Two possible fracture-line patterns are expected, depending on the h/L aspect ratio (Fig. 11b).

According to Roberts et al. [31], the generalized design bending moment m_d for full panels can be expressed as follows:

$$m_d = \alpha W \lambda_f L^2 \quad (16)$$

where α is the bending moment coefficient [31], Tables 8.4.1-21), which depends on: (i) the orthogonal ratio μ ; (ii) the aspect ratio h/L ; (iii) the boundary conditions. It should be noted that, to take into account the self-weight contribution when defining α , in [31] it is recommended that the orthogonal ratio is corrected as follows:

$$\mu = \frac{f_{kx} + \frac{\gamma h}{2} \lambda_m}{f_{ky}} \quad (17)$$

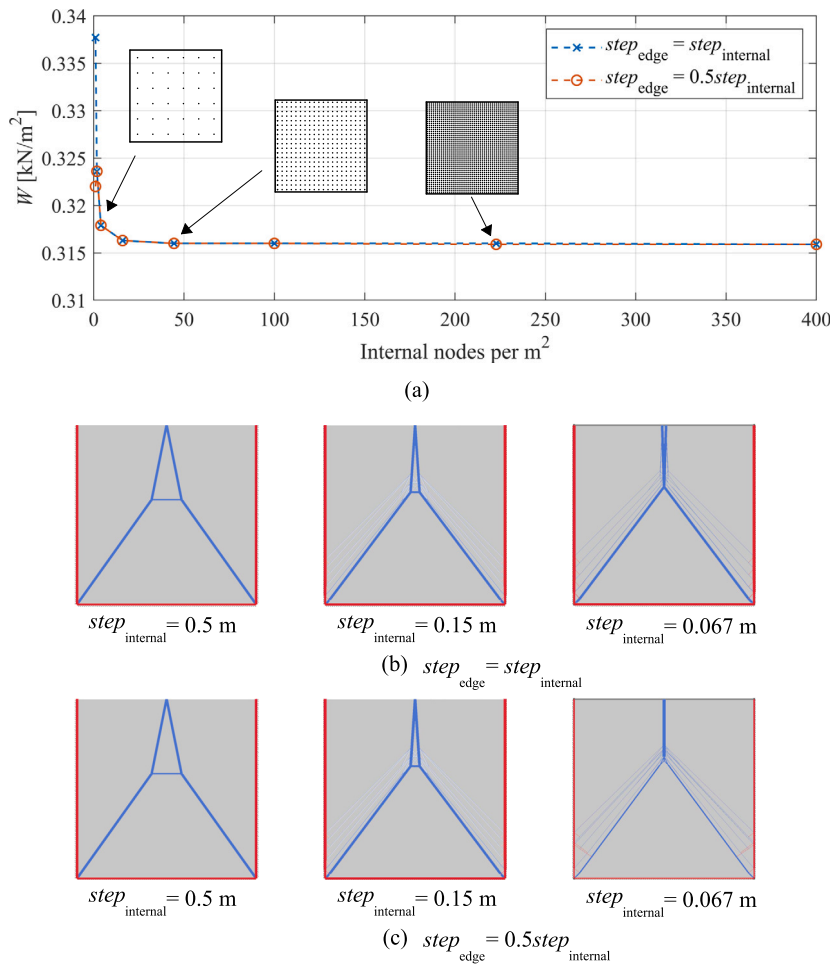


Fig. 9. Simply supported panel: (a) sensitivity of collapse load (W) to nodal spacing ($step$) and comparison for different refinement along edges; critical DLO yield-line pattern for (b) $step_{edge} = step_{internal}$ and (c) $step_{edge} = 0.5step_{internal}$.

where f_{kx} and f_{ky} are respectively the characteristic flexural tensile strength values in the x and y directions, $\frac{\gamma h}{2}$ represents the vertical stress at the mid-height of the panel, and where λ_m is the material partial safety factor. Also, the generalized design moment of resistance m_r can be stated as follows:

$$m_r = \frac{f_{ky} t^2}{\lambda_m 6} \quad (18)$$

By combining Eqs. (16) and (18), it is possible to determine the minimum thickness t required to sustain a given load, or to determine the maximum out-of-plane load capacity if the thickness is given. It is convenient here to express the load capacity as a function of a given thickness, since the latter depends on the size of the adopted masonry units as follows:

$$W = \frac{f_{ky} t^2}{6 \alpha \lambda_m \lambda_f L^2} \quad (19)$$

where W is the out-of-plane uniform pressure load at failure and λ_f represents the partial safety factor on the loading, with a value of at least 1.0 indicating that the structure is safe.

Results obtained for different wall aspect ratios are reported in Fig. 12; the reader is referred to Table 1 for values of the governing parameters.

It is clear that the results obtained using the analytical and DLO methods are in reasonably good agreement, with the maximum percentage difference being 2.12%, for the $h/L = 1.4$ case. (Note that

this discrepancy is principally a consequence of the approximate way in which self-weight effects are handled in the analytical model; e.g., whereas the vertical stress in reality varies with height, something that is captured in the DLO model, only the mid-height stress value is used in the analytical calculations.) The overall forms of the expected yield-line patterns are also approximately replicated via the DLO approach, e.g., when $h/L = 0.6$ (albeit the DLO solutions often also include secondary yield-lines, improving the solutions slightly).

4.2.2. Panel with weak base shear joint

The example shown in Fig. 13 is used to investigate the potential for shear failure occurring at the base of the wall, e.g., if there is a weak layer at the base of the wall due to the presence of a DPC.

To analyse this case, for the sake of simplicity consider a horizontal fracture line of unit length at height y . The strip above the fracture line, denoted A^* , also has unit length and height $h^* = h - y$. If the unit weight is γ , the vertical stress is $\sigma_y = \gamma(h - y)$ (assuming no additional vertical load is applied at the top of the wall). Given an out-of-plane load W , the shear and bending moment at the fracture line are respectively equal to $W(h - y)$ and $W(h - y)^2/2$. By using Eqs. (7a) and (13), it is possible to derive the load required to induce failure due to shear (W_t) or vertical flexure (W_{mx}):

$$\begin{aligned} W_t &= \frac{t}{h - y} f_v; \\ W_{mx} &= \frac{t^2}{3(h - y)^2} (f_x + \sigma_y) \end{aligned} \quad (20)$$

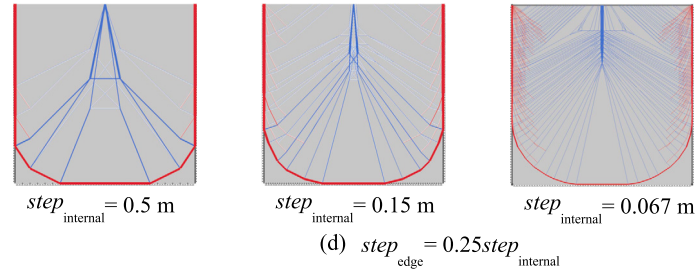
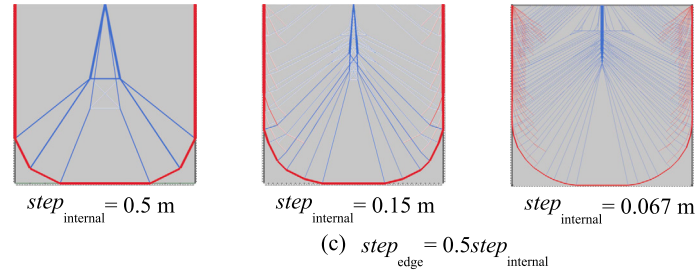
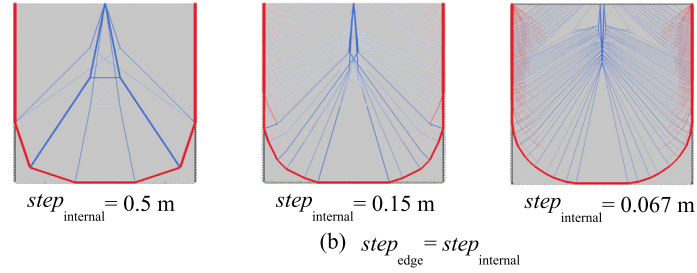
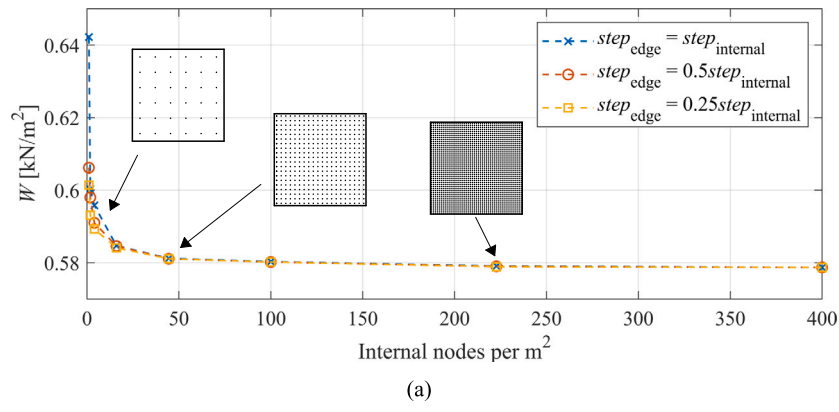


Fig. 10. Fixed panel: (a) sensitivity of collapse load (W) to nodal spacing ($step$) and comparison for different refinement along edges; critical DLO yield-line pattern for (b) $step_{edge} = step_{internal}$, (c) $step_{edge} = 0.5step_{internal}$, and (d) $step_{edge} = 0.25step_{internal}$.

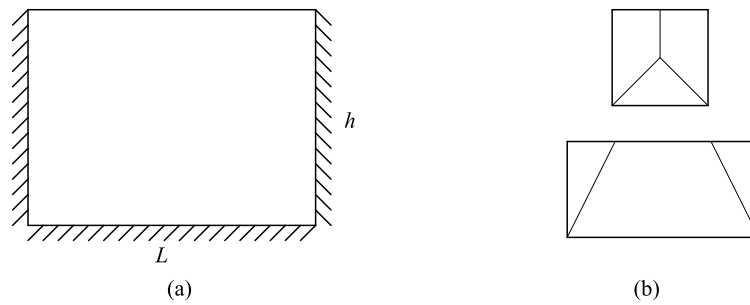


Fig. 11. Simply supported panel: (a) geometry and boundary conditions; (b) expected crack patterns.

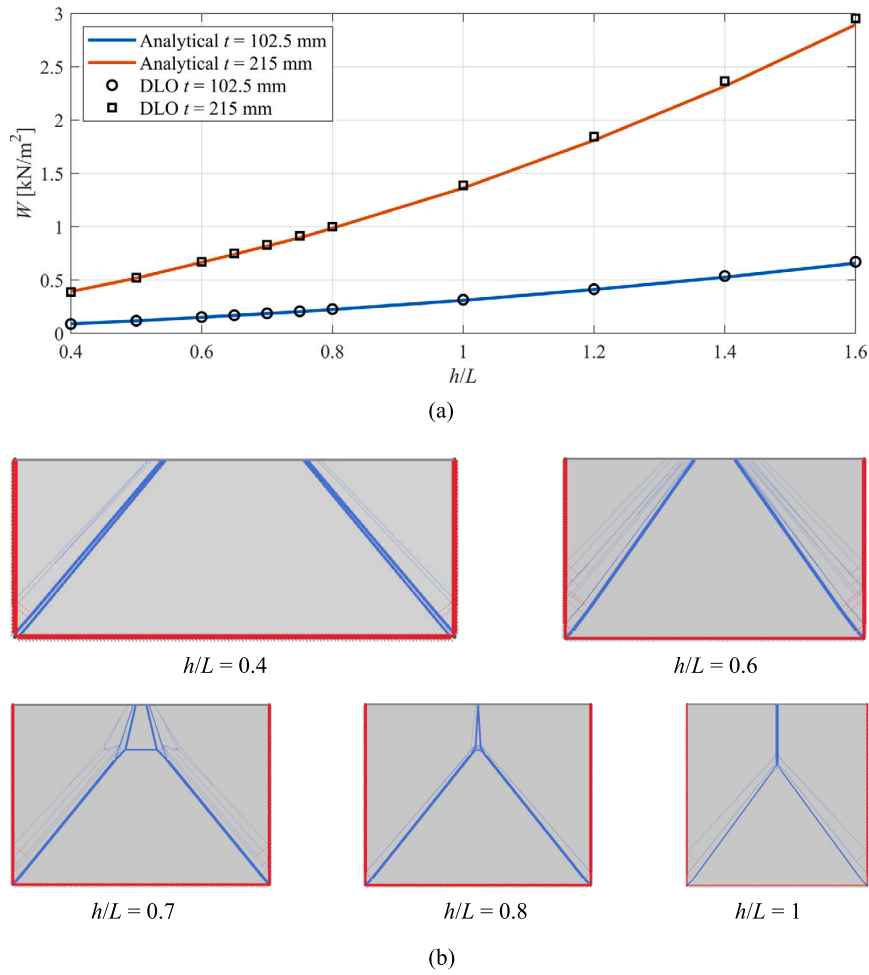


Fig. 12. Simply supported panel: (a) comparison of collapse load values obtained via analytic procedure [31] and DLO for different aspect ratios; (b) representative identified critical yield-line patterns.

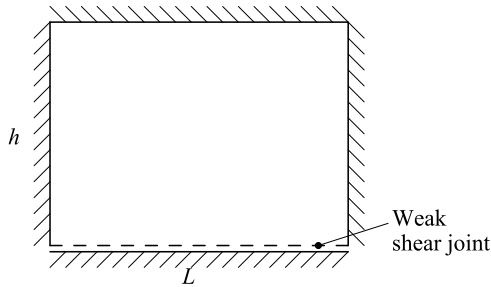


Fig. 13. Panel with weak base shear joint: geometry and boundary conditions.

where f_v is defined as described in Eq. (15). The components f_v and $(f_x + \sigma_y)$ are observed to be of the same order of magnitude. The ratio $\frac{t}{h-y}$ depends on the geometry and is typically below 1.0 in the case of a slender panel. Since W_{mx} is a function of the square of this ratio, this clearly indicates that slender panels are more vulnerable to bending failure.

In Fig. 14 values of W_t and W_{mx} , evaluated according to Eq. (20), are compared. Specifically, the ratio W_{mx}/W_t is given for a range of t/h ratios, taking $\gamma = 19 \text{ kN/m}^3$ and $f_x = f_{v0} = 0.1 \text{ MPa}$. It is evident that the ratio is generally lower than 1.0 except near the top of the wall panel. Also, it is clear that the ratio is higher when the slenderness of the panel is low (albeit a ratio of $t/h = 0.5$ would be unusual in practice).

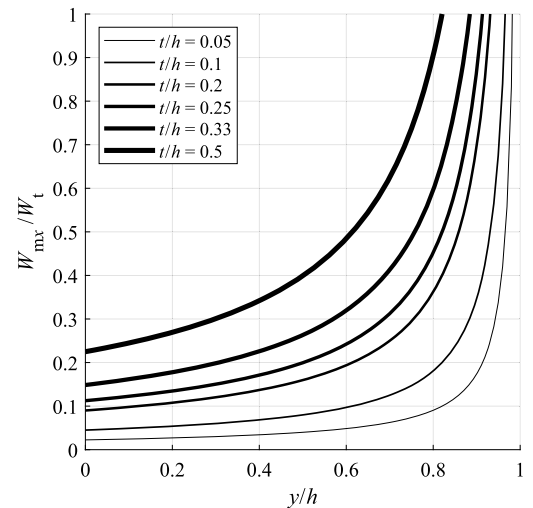


Fig. 14. Panel with weak base shear joint: W_{mx}/W_t for different values of t/h and y/h (assuming $\gamma = 19 \text{ kN/m}^3$; $f_x = f_{v0} = 0.1 \text{ MPa}$ throughout - i.e., no weak joint in this case).

However, as previously indicated, shear resistance will often be much lower in the region of a DPC positioned near the bottom of a wall.

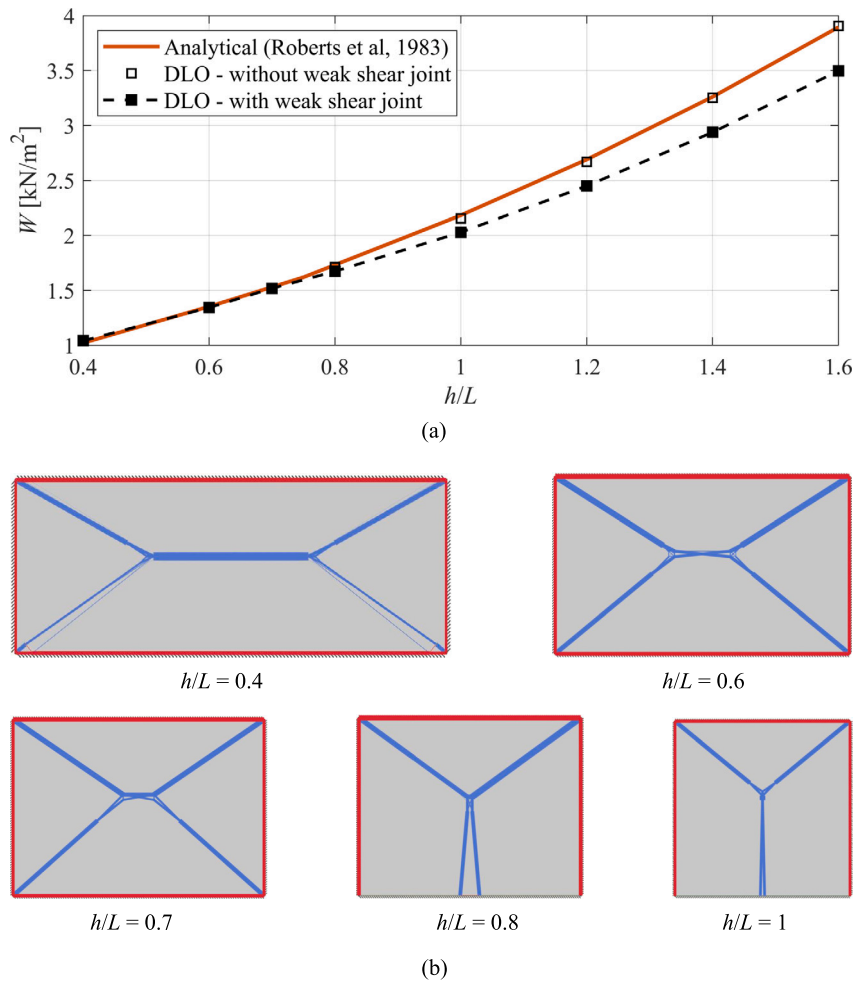


Fig. 15. Panel with weak base shear joint: (a) comparison of collapse load values obtained via analytical procedure [31] and DLO for different aspect ratios; (b) representative identified critical DLO yield-line patterns.

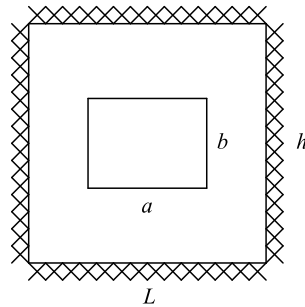


Fig. 16. Fixed wall panel with opening: geometry and boundary conditions.

In work presented by Mojsilovic in [56], it was found that DPC membranes can result in joints with very low shear-bond strength (e.g., 0.04 MPa) and/or coefficient of friction (e.g., 0.06). Also, a partial safety factor of 2.5 may typically be applied when determining the design shear resistance. Thus it seems justified to here assume a very weak shear joint at the bottom edge of the wall; a limit on the shear of 0.01 MPa has therefore been assumed. Fig. 15 shows DLO analysis results for various wall aspect ratios, considering a constant wall height (as in Section 4.2.1). In Fig. 15(a) results are compared to those corresponding to walls without a weak joint, obtained both via DLO and via the analytical model proposed in [31]. From the results obtained it is evident that no shear failures are observed for low aspect ratios, with the failure mechanisms

in this case governed by flexural yield-lines. However, when $h/L \geq 0.8$, out-of-plane displacements occur at the bottom edge. The maximum reduction of out-of-plane resistance has in this case found to be 10.5%, though larger differences would be observed in the case of thicker wall panels.

4.2.3. Fixed panel with opening

Now consider a single-leaf wall panel containing a central opening, with fixed supports along its four external edges. As with the previous case, the size of the opening is parameterized with horizontal and vertical dimensions equal to a and b respectively; see Fig. 16. Here two scenarios are considered: (i) the surface load is applied only to the wall

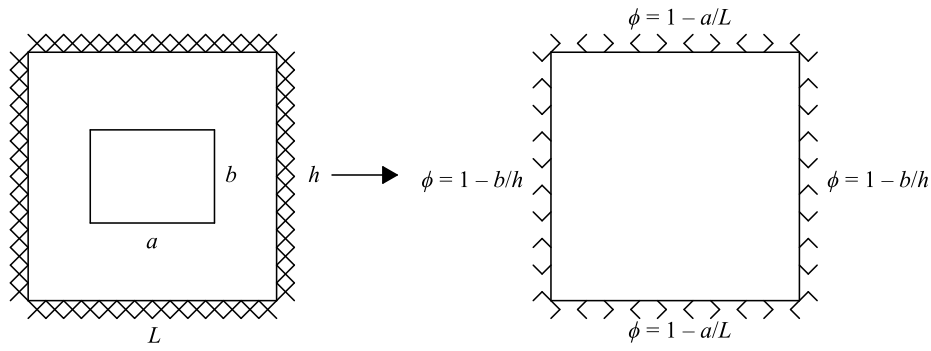


Fig. 17. Fixed panel with opening: conceptual scheme of the analytical method proposed in [31] in the case of a small opening.

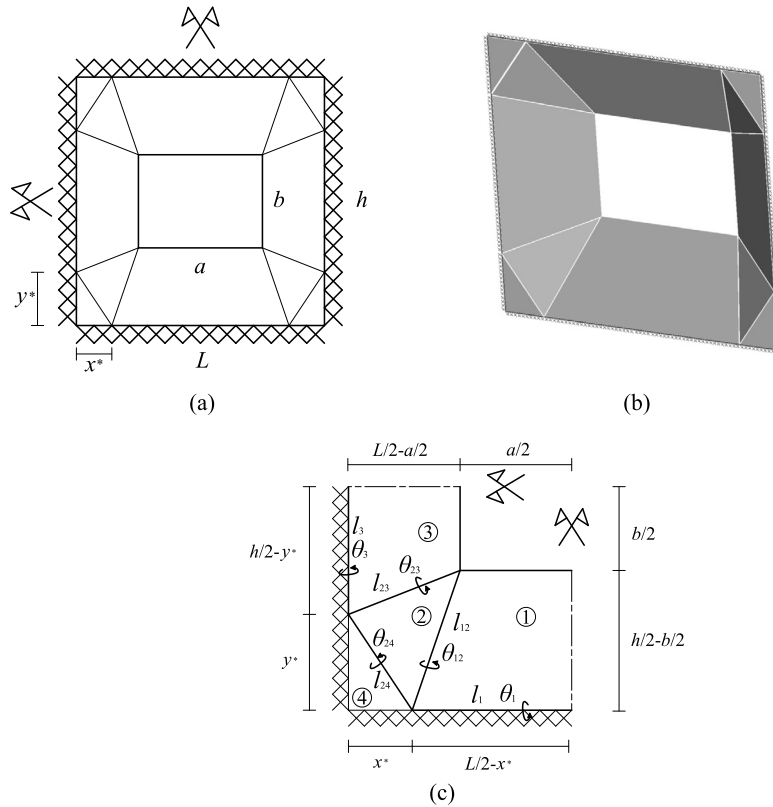


Fig. 18. Fixed panel with opening - predetermined critical yield-line pattern: (a) overall geometry and boundary conditions; (b) associated deformed failure mechanism; and (c) detail of the geometrical quantities involved in the analysis.

area (i.e., $hL - ab$), corresponding to the case when a horizontal body force derived from an earthquake is applied; (ii) the surface load is applied to the full enclosed area (i.e., hL), corresponding to the case when wind load is applied to a ‘window and frame system’, which can transmit shear to the boundaries of the opening. In the analysis, the second scenario can be modelled by assigning additional out-of-plane line loads to the boundaries of the opening.

Whichever scenario is considered, according to Roberts et al. [31] and Johansen [7], an approximated solution for the panel with opening can be obtained from Eq. (19), on the assumption that: (i) the size of the opening is small; and (ii) the fixity of each edge is reduced proportionally to the corresponding dimension of the opening (as shown in Fig. 17). Note however that for the ‘small opening’ case some details are missing, such as whether or not the load is assumed to be applied to the full enclosed area. Thus an additional reference solution is employed here to permit direct comparison with the DLO results. As suggested by

Johansen [7], this reference solution is based on an *a priori* definition of the yield-line pattern, with an evaluation of the associated ultimate load established by balancing the external and internal work; the associated equations are reported in Appendix A. However, this strategy can be a useful alternative to Eq. (19) when the opening cannot be considered small (i.e., for an opening between 5–25% of the panel area). The hypothesized yield-lines pattern design is depicted in Fig. 18, where geometrical parameters x^* and y^* must be determined via optimization. The evaluation of such a mechanism through minimization of the load factor, as a function of x^* and y^* (see Appendix A for details), has been computed here using a simple MATLAB [62] script.

Unlike the examples considered in Section 4.2.1, here the overall size of the panel has been kept constant, whereas the opening dimensions have been varied (see Table 1). The opening has initially been assumed to have a 1:1 aspect ratio, with the opening area varied between 0.4% and 25% of the full area. Moreover, to facilitate direct

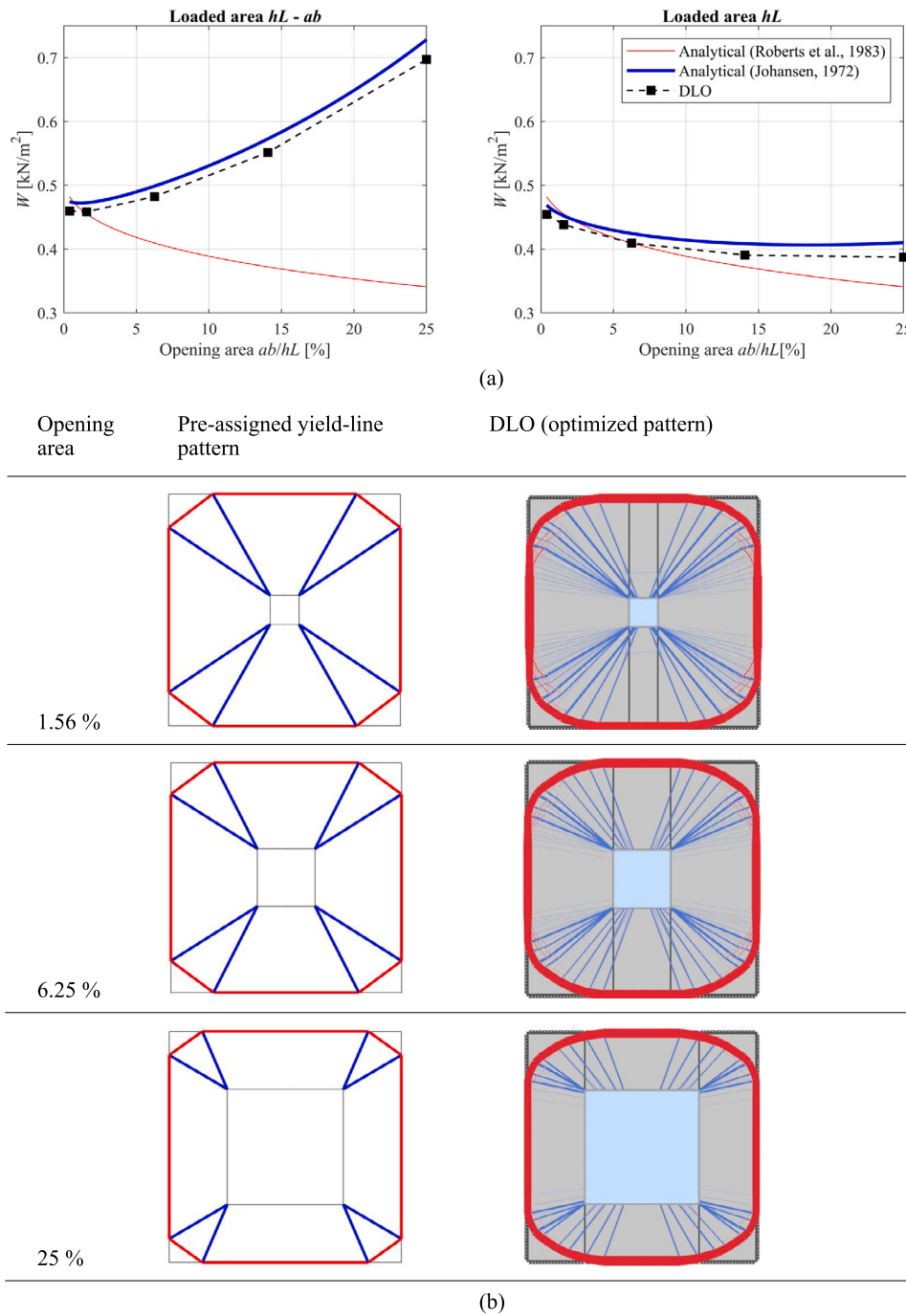


Fig. 19. Fixed panel with opening - results for $h/L = 1$, $a/b = 1$, $0 < ab \leq 0.5hL$, with self-weight effects neglected: (a) comparison of collapse load values; (b) comparison of critical yield-line patterns for various opening sizes (expressed as a % of the enclosed wall area).

comparison with the equations reported in Appendix A, self-weight has initially been neglected in both the analytical and numerical models. Results are presented in Fig. 19.

It is evident from Fig. 19a that the DLO solutions follow a similar trend to Johansen's, but since they correspond to more refined yield-line layouts, they are more conservative. On the other hand, the [31] solutions obtained via Eq. (19) follow a markedly different trend for the first load condition considered (involving applying body forces), though a more similar one for the second (involving wind pressures). This is likely because the approximations underpinning the method are inappropriate in the former case, when the opening size is not negligible.

Next, results obtained when self-weight effects are now included, for a range of opening aspect ratios, are presented in Fig. 20. It is evident that the DLO solutions are still generally similar to Johansen's, though are more conservative since the corresponding failure mechanisms are more accurate. Larger differences are observed for smaller opening aspect ratios, e.g., the $a/b = 0.25$ case. Again, this is reflective of the more accurate yield-line patterns obtained via DLO, compared with the pre-assigned pattern.

4.3. Chong's walls

The example walls studied in this section have been selected from the experimental programme of tests presented by [32] and [63]. Here

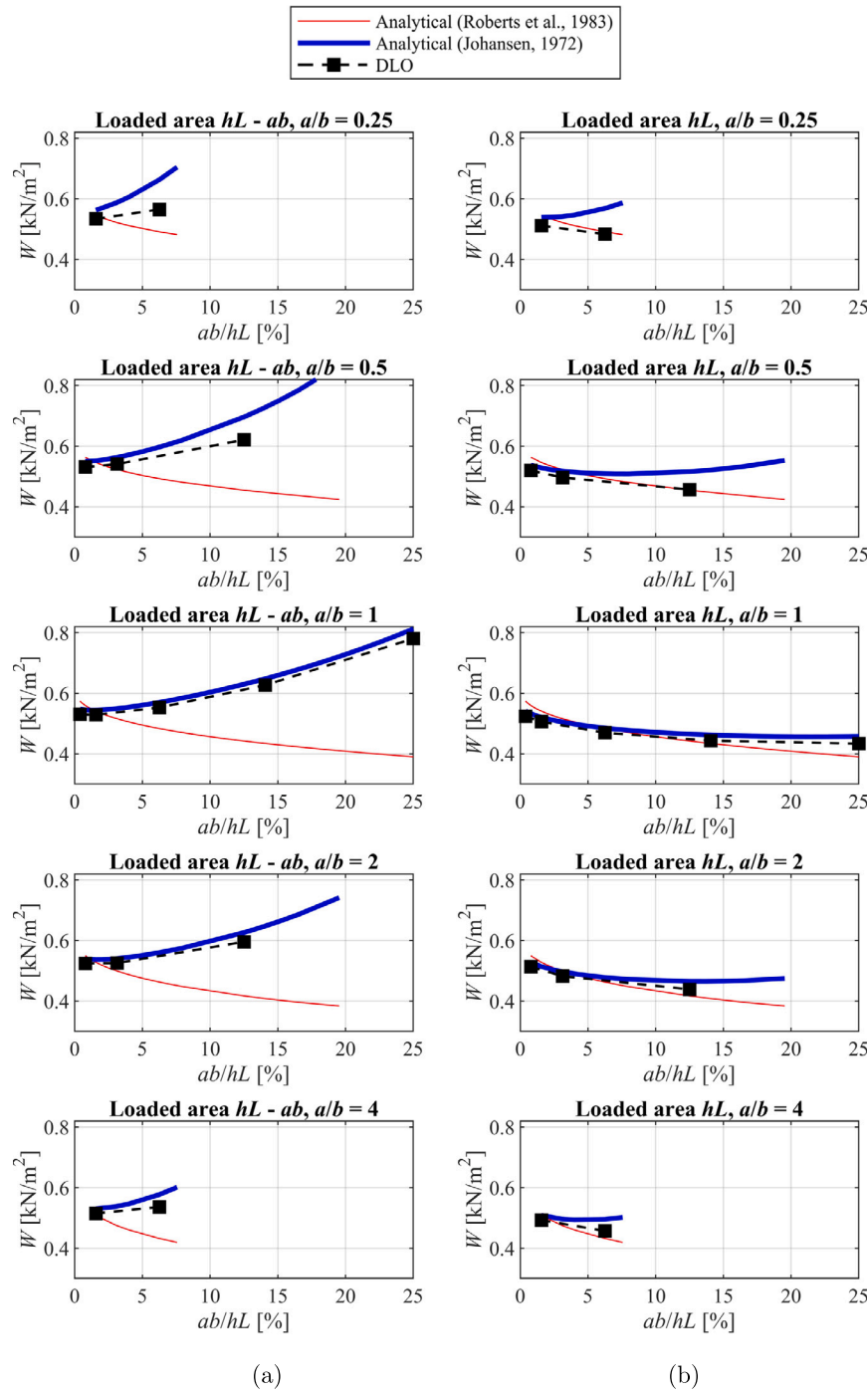


Fig. 20. Fixed panel with opening: (a) capacity W when only wall area loaded; (b) capacity W when full enclosed area loaded. Results shown for $h/L = 1, 0.25 \leq a/b \leq 4, 0 < ab \leq 0.5hL$.

a selection of the single leaf, stretcher bonded ('SB') walls described by Chong are used as benchmarks for the DLO limit analysis procedure; these walls have also been used to validate other numerical models in recent years (e.g., [42,64,43,65,66,48,67,68]). The geometry and boundary conditions of the walls are shown in Fig. 21. According to [32], these test wall panels were built using Class B bricks; flexural strengths were determined from experiments and are presented in Table 1.

When compared with experimental results, approaches based on yield-line theory can be expected to overestimate the collapse load somewhat, even if the collapse mechanism is well represented. This is not only because the kinematic multiplier is by definition an upper

bound on the actual collapse multiplier, but also due to the quasi-brittle behaviour of masonry [13]. This contrasts with the perfect plasticity assumed at flexural hinges according to yield-line theory, and which is a hypothesis that is fundamental to the formal limit analysis theorems of plasticity. No attempt to model post-cracking behaviour has been made here, e.g., as was recently undertaken using a non-linear kinematic analysis in [15]. Also, whereas a fixed boundary was indicated to be present at the bases of the experimental walls (in [32] it is suggested that rotation at the bottom edge of each wall was constrained by filling the gaps between the sides of steel channel sections and the masonry with mortar), the likelihood of the bottom edge being capable of transmitting the full plastic moment in practice appears low. Thus a

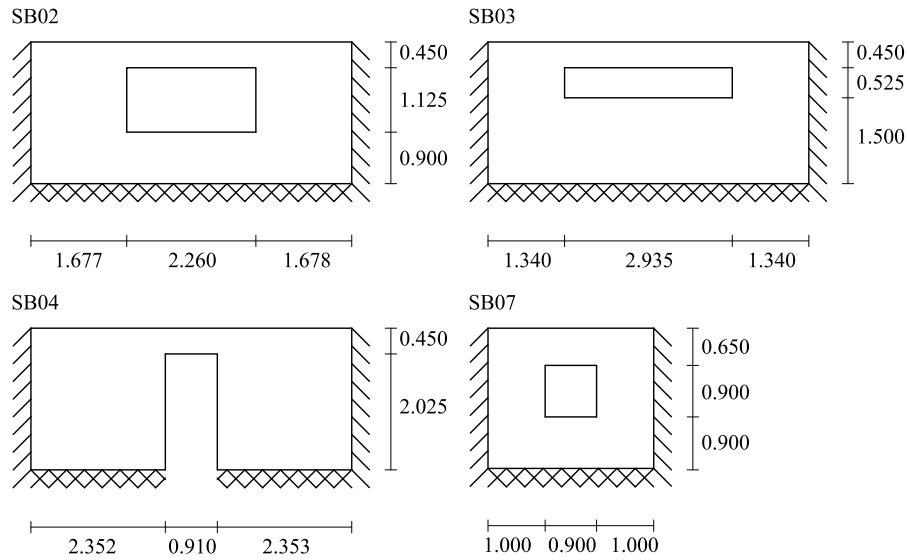


Fig. 21. Chong's walls: geometry and boundary conditions of selected wall panels. All dimensions in metres (after [32]).

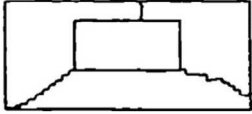


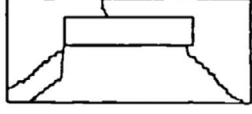


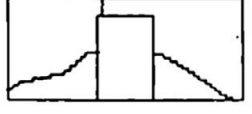
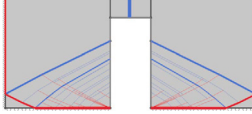
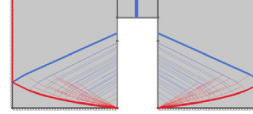

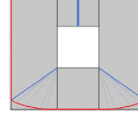
Experimental (Chong, 1993)	DLO Vertically supported, $\phi = 0.5$ at the bottom	DLO Vertically supported, fixed at the bottom
SB02  $W = 2.4 \text{ kN/m}^2$	 $W = 2.459 \text{ kN/m}^2$ $\text{diff} = 2.46 \%$	 $W = 2.854 \text{ kN/m}^2$ $\text{diff} = 18.92 \%$
SB03  $W = 2.3 \text{ kN/m}^2$	 $W = 2.23 \text{ kN/m}^2$ $\text{diff} = -3.04 \%$	 $W = 2.49 \text{ kN/m}^2$ $\text{diff} = 8.26 \%$
SB04  $W = 2.2 \text{ kN/m}^2$	 $W = 2.39 \text{ kN/m}^2$ $\text{diff} = 8.64 \%$	 $W = 2.566 \text{ kN/m}^2$ $\text{diff} = 16.64 \%$
SB07  $W = 5.5 \text{ kN/m}^2$	 $W = 5.547 \text{ kN/m}^2$ $\text{diff} = -0.78 \%$	

Fig. 22. Chong's walls: example failure mechanisms from [32], shown with the corresponding DLO results. Corresponding out-of-plane loads at failure W are shown, with differences between DLO and experimental loads indicated.

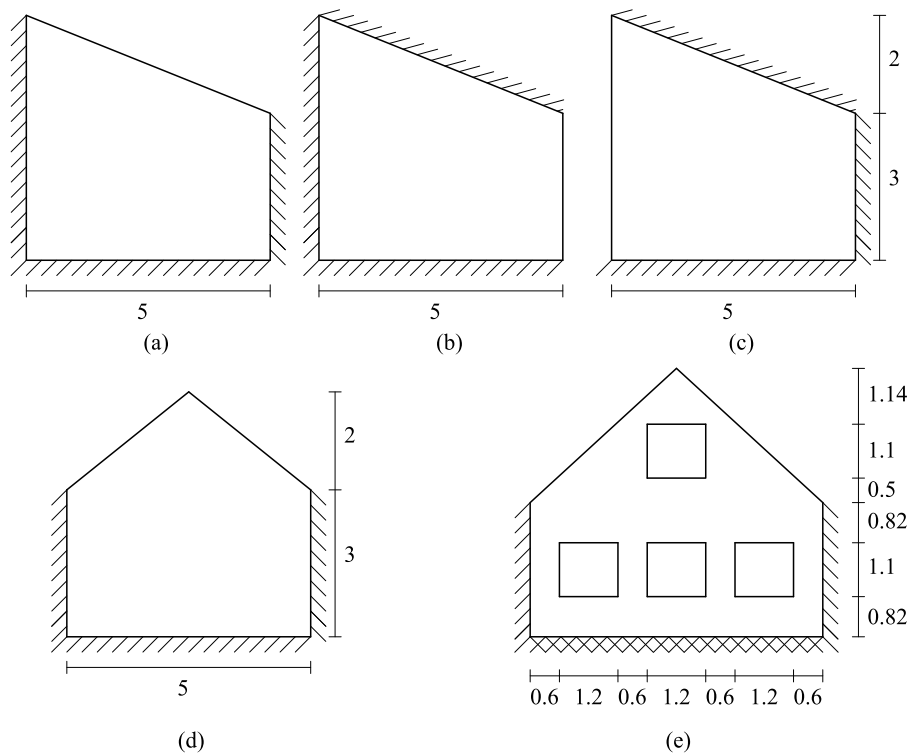


Fig. 23. Gable walls - geometry and boundary conditions: (a-c) walls with various boundary conditions; (d) wall with pitch; (e) wall with pitch and multiple openings. All dimensions are in metres.

partial base fixity case was also considered in the numerical analyses undertaken, in addition to the fully fixed case. Results obtained using the DLO analysis model are presented in Fig. 22 along with corresponding experimental results, considering both collapse loads and fracture-line patterns.

It can be observed from Fig. 22 that reasonably close estimates of the experimental load can be obtained when the bottom edge is assumed to be partially fixed, with a maximum difference between experimental and numerical load values of 8.64%, occurring in the case of wall SB04. The yield-line patterns were also found to be in better agreement with the experimentally observed fracture-lines when the bottom edge was assumed to be partially fixed. Note that all walls were observed to fail via formation of flexural fracture-lines, with no shear or torsional failures observed, either experimentally or in the numerical models. However, as expected, there are clearly some differences between the experimental and numerical results. One issue is that in the DLO model the bending resistance of an inclined yield-line (Eq. (11)) is analytically defined without taking the actual masonry texture into account; the development of a homogenized DLO model for the out-of-plane behaviour of masonry is currently a work in progress.

4.4. Gable walls

In this section, various wall panels with more complex geometries are considered. Specifically, taking inspiration from the geometries of walls frequently encountered in the UK, various gable wall examples are considered in order to further explore the range of applicability of the proposed DLO modelling approach.

The adopted gable wall geometries are presented in Fig. 23; the flexural strength values and partial safety factors adopted in Section 4.2.1 are again assumed here (see Table 1). The walls shown in Fig. 23(a)-(d) are assumed to be 102.5 mm thick, whereas the wall in Fig. 23e is assumed to be 215 mm thick.

Firstly, results obtained from the analysis of the walls presented in Fig. 23(a)-(d) are compared with those obtained using the analytical

model proposed in [31]. However, in the latter case, due to the nature of the geometry, Eq. (19) is applied by assuming an equivalent rectangular domain characterized by an average value of h , following the suggestion made in [31]. Results are presented in Fig. 24. It is evident that whereas in the case of the walls presented in Fig. 23(a) and (d), the differences between the experimental and analytical collapse loads are quite small (with a 3.9% lower collapse load value provided by DLO in the case of the wall presented in Fig. 23(d)), in the case of the walls presented in Fig. 23(b) and (c) the differences are larger (with a 19.4% lower collapse load value provided by DLO in the case of the wall presented in Fig. 23(c)).

Secondly, the wall presented in Fig. 23(e) is considered. In this case, given the presence of multiple openings, it is not possible to apply a simple analytical model with confidence. In contrast, the automated DLO procedure can be applied to problems of arbitrary geometry without difficulty. For this problem a nodal spacing of 0.067 m is again employed, leading to a discretization comprising 5967 nodes in total. Results are presented in Fig. 25, with the load either applied only to the exposed wall area or to the full enclosed area; the corresponding collapse loads are 0.311 and 0.259 kN/m² respectively. The corresponding yield-line patterns are almost identical. No shear or torsional failures are evident.

It is worth noting that although the failure mechanism obtained for the wall presented in Fig. 23(e) turned out to be relatively simple, and therefore possible to analyse by hand, identifying this by hand via a trial-and-error procedure would nevertheless be challenging for a geometry of this complexity, with a non-conservative estimate of load capacity obtained if the critical mechanism was missed. The proposed DLO approach avoids this by automatically identifying the critical yield-line pattern and the associated load multiplier, with the process taking a matter of a few seconds on a modern desktop PC.

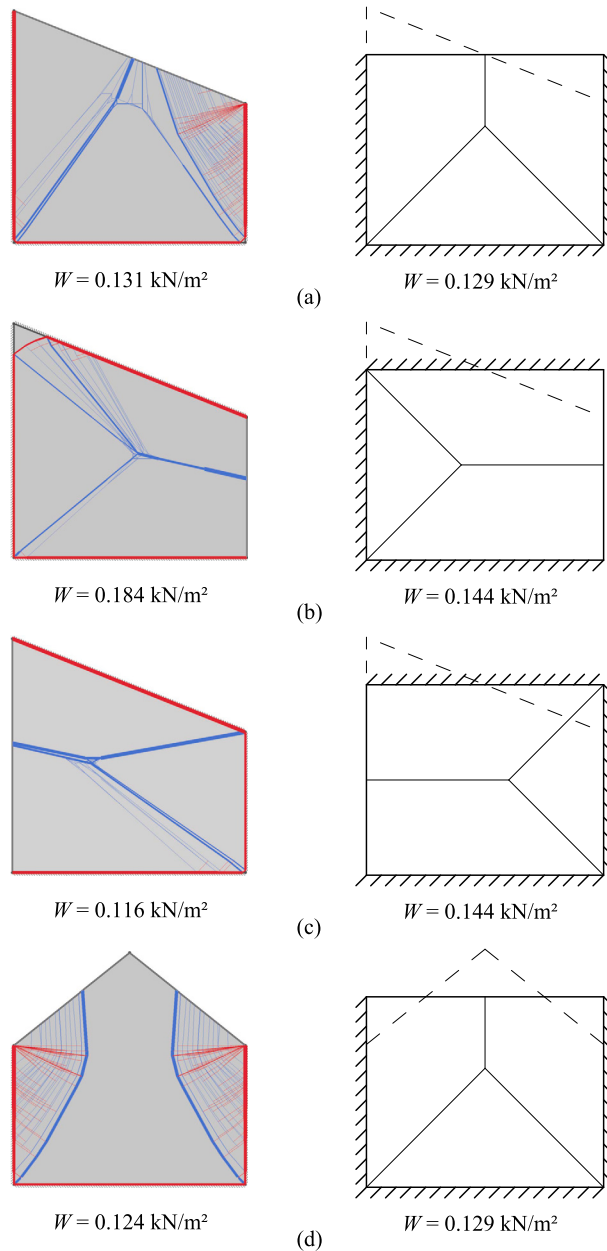


Fig. 24. Gable walls, cases (a)-(d): predicted DLO failure mechanisms (left) and corresponding analytically assumed mechanisms (right), applied using an equivalent geometry (after [31]; the extents of the actual geometries are indicated by dashed lines). Corresponding out-of-plane loads at failure W are also indicated.

5. Conclusions

A new limit analysis procedure for computing the maximum out-of-plane load that can be sustained by masonry cladding panels has been presented. This uses the powerful discontinuity layout optimization (DLO) procedure, previously successfully applied to various other engineering problems. With DLO, a given problem is discretized using nodes interconnected by potential yield-lines. Three kinematic variables are assigned to each: normal rotation, twisting rotation and shear displacement. This results in a linear programming (LP) problem where the objective is to identify the multiplier on the applied out-of-plane loading, balancing external and internal work and evaluating internal energy dissipation using the hypothesis of perfect plasticity. Solving the LP problem furnishes a set of values for the kinematic variables, with non-zero values corresponding to active fracture lines in the critical failure mechanism, together with the collapse load multiplier.

The proposed method involves enriching classical yield-line theory, which describes the failure mode in terms of mutual normal rotations only, by also including possible shear and torsional failures. The main mechanical properties of masonry are taken into account by defining plastic moment and shear capacities as functions of the vertical load. Plastic moment capacity calculations can be modified to account for the presence of double-leaf or hollow block masonry panels. Moreover, the procedure is fully automatic and suitable for application to highly irregular geometries.

Several example problems have been used to demonstrate the efficacy and potential of the DLO analysis procedure, including wall problems also solved via analytical means, walls tested in the laboratory, and more geometrically complex gable walls containing multiple openings. The DLO solutions obtained have been found to be in good agreement with analytical solutions, except in cases where approximations inherent in the latter furnished over-conservative results. Generally reasonable

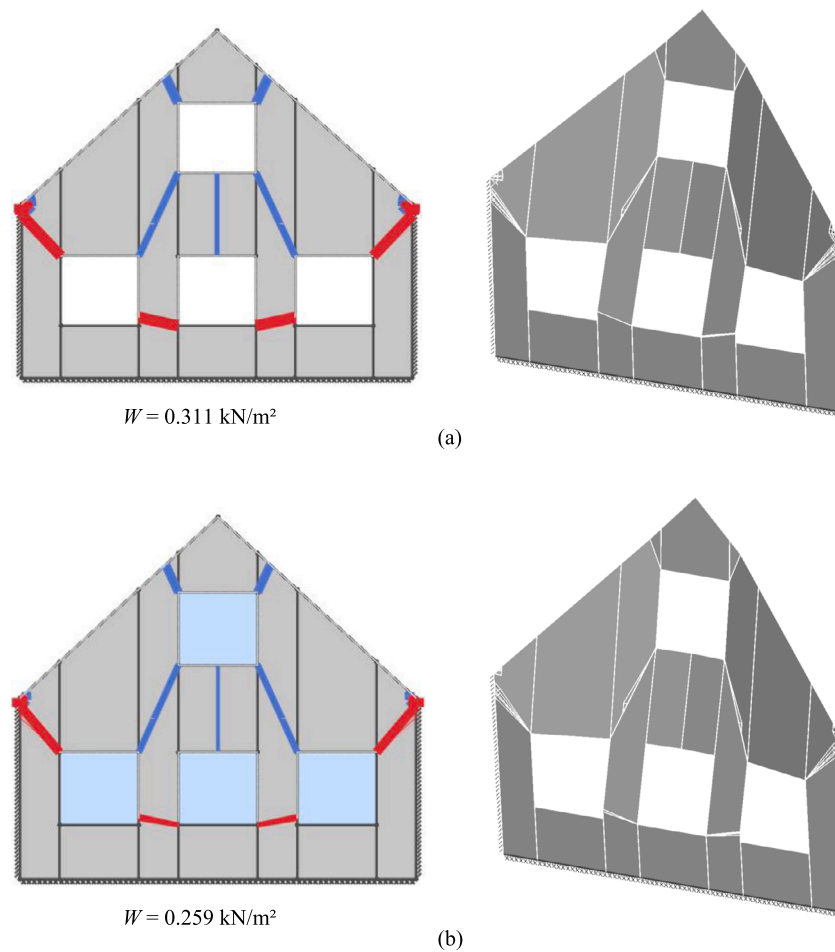


Fig. 25. Gable wall with multiple openings: (a) critical yield-line patterns and associated deformed failure mechanisms when only the wall-area is loaded; (b) situation when the full gable area is loaded. Corresponding out-of-plane loads at failure W are also indicated.

agreement with experimental results was also observed. Finally, when applied to the analysis of irregular gable wall geometries, it was observed that the DLO procedure makes it possible to model problems that are difficult, if not impossible, to analyse via traditional hand analysis methods.

Future research will focus on applying the DLO procedure to the out-of-plane analysis of historic masonry structures, where the bond strength of the mortar adhering the masonry units may be very low or non-existent. For such cases, homogenization techniques capable of taking account of the actual masonry texture will be employed, with both planar and curved masonry elements considered.

CRediT authorship contribution statement

Nicola Grillanda: Writing – review & editing, Writing – original draft, Methodology, Investigation. **Linwei He:** Writing – review & editing, Software, Methodology, Conceptualization. **Matthew Gilbert:** Writing – review & editing, Supervision, Software, Methodology, Funding acquisition, Conceptualization. **Colin C. Smith:** Writing – review & editing, Supervision, Methodology.

Declaration of competing interest

The authors declare the following financial interests/personal relationships which may be considered as potential competing interests: Matthew Gilbert reports financial support was provided by Engineering and Physical Sciences Research Council, under grant reference EP/T001305/1. Colin Smith reports financial support was provided

by Engineering and Physical Sciences Research Council, under grant reference EP/T001305/1. Matthew Gilbert reports a relationship with LimitState Ltd that includes: board membership and equity or stocks. Colin Smith reports a relationship with LimitState Ltd that includes: board membership and equity or stocks. Matthew Gilbert has patent #U.S. patent 8,140,175 issued to University of Sheffield. Colin Smith has patent #U.S. patent 8,140,175 issued to University of Sheffield. If there are other authors, they declare that they have no known competing financial interests or personal relationships that could have appeared to influence the work reported in this paper.

Acknowledgements

The authors acknowledge the financial support provided by the Engineering and Physical Research Council, under grant reference EP/T001305/1.

Appendix A. Johansen's equations for a domain with an opening

Consider a square domain with a rectangular opening, where, for the sake of simplicity, the presented equations refer to the case where self-weight is neglected. Thus, the panel can be considered to be symmetrical about two orthogonal axes, with the analysis reduced to a quarter of the actual domain (see Fig. 18c):

$$\begin{aligned}
 B_1 &= L - a, & B_2 &= L + 2a - 2x^*, \\
 B_3 &= L + a - 2x^*, & B_4 &= L - a - 2x^* \\
 C_1 &= h - b, & C_2 &= h + 2b - 2y^*, \\
 C_3 &= h + b - 2y^*, & C_4 &= h - b - 2y^* \\
 D &= \sqrt{x^{*2} + y^{*2}}
 \end{aligned} \tag{A.1a}$$

$$A_1 = \frac{C_1 B_3}{8}, A_2 = \frac{y^* B_1 + x^* C_1 - 2x^* y^*}{4}, A_3 = \frac{B_1 C_3}{8} \tag{A.1b}$$

$$\delta_1 = \frac{\bar{\delta} B_2}{3 B_3}, \delta_2 = \frac{\bar{\delta}}{3}, \delta_3 = \frac{\bar{\delta} C_2}{3 C_3} \tag{A.1c}$$

$$\theta_1 = \frac{2\bar{\delta}}{C_1}, \theta_{24} = \frac{2\bar{\delta} D}{y^* B_1 + x^* C_1 - 2x^* y^*}, \theta_3 = \frac{2\bar{\delta}}{B_1}, \tag{A.1d}$$

$$\theta_{12} = \theta_1 \cos\left(\arctan\left(\frac{C_1}{B_4}\right)\right) - \theta_{24} \cos\left(\pi - \arctan\left(\frac{C_1}{B_4}\right) - \arctan\left(\frac{y^*}{x^*}\right)\right), \tag{A.1e}$$

$$\theta_{23} = \theta_3 \cos\left(\arctan\left(\frac{B_1}{C_4}\right)\right) - \theta_{24} \cos\left(\pi - \arctan\left(\frac{B_1}{C_4}\right) - \arctan\left(\frac{x^*}{y^*}\right)\right) \tag{A.1f}$$

$$m_{12} = \frac{m_{px} B_4^2 + m_{py} C_1^2}{B_4^2 + C_1^2}, m_{23} = \frac{m_{px} C_4^2 + m_{py} B_1^2}{C_4^2 + B_1^2}, m_{24} = \frac{m_{px} x^{*2} + m_{py} y^{*2}}{D^2} \tag{A.1g}$$

$$l_1 = \frac{L}{2} - x^*, l_{12} = \frac{1}{2} \sqrt{B_4^2 + C_1^2}, l_{23} = \frac{1}{2} \sqrt{C_4^2 + B_1^2}, \tag{A.1h}$$

$$l_{24} = D, \quad l_3 = \frac{h}{2} - y^* \tag{A.1i}$$

$$\begin{aligned}
 \{x^*, y^*\} &= \arg \min W \\
 &= \frac{m_{px} \theta_1 l_1 + m_{12} \theta_{12} l_{12} + m_{23} \theta_{23} l_{23} + m_{24} \theta_{24} l_{24} + m_{py} \theta_3 l_3}{A_1 \delta_1 + A_2 \delta_2 + A_3 \delta_3 + ab\bar{\delta}/4}
 \end{aligned} \tag{A.1j}$$

where the constants in (A.1a) have been introduced to simplify the subsequent expressions, and $\bar{\delta}$ is the maximum out-of-plane displacement assigned along the opening perimeter. The quantity $ab\bar{\delta}/4$ in the denominator of the objective function represents the work done by the unit surface load applied to the opening perimeter, which is omitted for some load cases. By varying the geometrical parameters x^* and y^* the minimum load factor can be determined, achieved here by using a specially written MATLAB [62] script. The results obtained provide analytical benchmarks against which DLO solutions can be compared.

Data availability

Data will be made available on request.

References

- [1] Chiozzi A, Miranda E. Fragility functions for masonry infill walls with in-plane loading. *Earthq Eng Struct Dyn* 2017;46(15):2831–50.
- [2] Heyman J. The stone skeleton. *Int J Solids Struct* 1966;2(2):249–79.
- [3] Heyman J. Leaning towers. In: *Masonry construction: structural mechanics and other aspects*; 1992. p. 153–9.
- [4] Giuffrè A. Sicurezza e conservazione dei centri storici: il caso Ortigia: codice di pratica per gli interventi antisismici nel centro storico. Laterza; 2000.
- [5] Wang P, Milani G. Seismic vulnerability prediction of masonry aggregates: iterative finite element upper bound limit analysis approximating no tensile resistance. *Eng Struct* 2023;293:116595.
- [6] Wang P, Milani G. Specialized 3d distinct element limit analysis approach for a fast seismic vulnerability evaluation of massive masonry structures: application on traditional pagodas. *Eng Struct* 2023;282:115792.
- [7] Johansen KW. Yield-line formulae for slabs. *Leatherhead: Eyre & Spottiswoode Publications Limited*; 1972.
- [8] CP111. *Structural recommendations for load-bearing walls*. London: British Standards Institution; 1970.
- [9] CP121. *Code of practice for walling. Part 1: brick and block masonry*. London: British Standards Institution; 1973.
- [10] BS5628. *Code of practice for the structural use of masonry. Part 1: unreinforced masonry*. London: British Standards Institution; 1978.

- [11] BS-EN1996. *Eurocode 6 - design of masonry structures. Part 3: simplified calculation methods for unreinforced masonry structures*. London: British Standards Institution; 2006.
- [12] Hognestad E. Yield-line theory for the ultimate flexural strength of reinforced concrete slabs. *ACI J Proc* 1953;49(3):637–56.
- [13] Lourenço PB. Analysis of historical constructions: from thrust-lines to advanced simulations. In: Lourenço PB, Roca P, editors. *Historical constructions*. University of Minho; 2001. p. 91–116.
- [14] Jäger W, Baker T. Critical remarks to the application of the yield line method on masonry. In: *Proceedings of the 11th Canadian masonry symposium*. Hamilton, Ontario Toronto: McMaster University/Canada Masonry Design Centre; 2009. p. 177–89.
- [15] Scacco J, Grillanda N, Milani G, Lourenço PB. Novel non-linear static numerical model for curved masonry structures based on a combined adaptive limit analysis and discrete FE computations. *Int J Solids Struct* 2022;236:111265.
- [16] Sinha BP. A simplified ultimate load analysis of laterally loaded orthotropic model brickwork panels of low tensile strength. *Struct Eng* 1978;56B(4):81–4.
- [17] Sinha BP. An ultimate load analysis of laterally loaded brickwork panels. *Int J Masonry Constr* 1980;1(2):57–61.
- [18] Drysdale RG, Essawy AS. Out-of-plane bending of concrete block walls. *J Struct Eng* 1988;114(1):121–33.
- [19] Chang L-Z, Messali F, Esposito R. Capacity of unreinforced masonry walls in out-of-plane two-way bending: a review of analytical formulations. *Structures* 2020;28:2431–47.
- [20] Pradhan B, Zizzo M, Sarhosis V, Cavaleri L. Out-of-plane behaviour of unreinforced masonry infill walls: review of the experimental studies and analysis of the influencing parameters. *Structures* 2021;33:4387–406.
- [21] Jones LL. *Ultimate load analysis of reinforced and prestressed concrete structures*. Interscience Publishers; 1962.
- [22] Jones LL, Wood RH. *Yield-line analysis of slabs*. Thames & Hudson; 1967.
- [23] Smith C, Gilbert M. Application of discontinuity layout optimization to plane plasticity problems. *Proc R Soc A, Math Phys Eng Sci* 2007;463(2086):2461–84.
- [24] Gilbert M, He L, Smith CC, Le CV. Automatic yield-line analysis of slabs using discontinuity layout optimization. *Proc R Soc A, Math Phys Eng Sci* 2014;470(2168):20140071.
- [25] Fishburn CC. *Effect of mortar properties on strength of masonry*, vol. 36. US Department of Commerce, National Bureau of Standards; 1961.
- [26] Willis CR. *Design of unreinforced masonry walls for out-of-plane loading*. PhD thesis. University of Adelaide; 2004.
- [27] Willis CR, Griffith MC, Lawrence SJ. Moment capacities of unreinforced masonry sections in bending. *Aust J Struct Eng* 2006;6(2):133–46.
- [28] Griffith M, Vaculik J. Out-of-plane flexural strength of unreinforced clay brick masonry walls. *TMS J* 2007;25(1):53–68.
- [29] Griffith MC, Vaculik J, Lam NTK, Wilson J, Lumantarna E. Cyclic testing of unreinforced masonry walls in two-way bending. *Earthq Eng Struct Dyn* 2007;36(6):801–21.
- [30] Liberatore L, AlShawa O. On the application of the yield-line method to masonry infills subjected to combined in-plane and out-of-plane loads. *Structures* 2021;32:1287–301.
- [31] Roberts JJ, Tovey AK, Cranston W, Beeby AW. *Concrete masonry designer's handbook*. Eyre & Spottiswoode Publications Ltd; 1983.
- [32] Chong VL. *The behaviour of laterally loaded masonry panels with openings*. PhD thesis. University of Plymouth; 1993.
- [33] Hendry AW. Lateral strength of unreinforced brickwork. *Struct Eng* 1973;51(2):43–50.
- [34] Haseltine BA, West HWH, Tutt JN. Design of walls to resist lateral loads. *Struct Eng* 1977;55(10):422–30.
- [35] Baggio C, Trovalusci P. Collapse behaviour of three-dimensional brick-block systems using non-linear programming. *Struct Eng Mech* 2000;10(2):181.
- [36] Casolo S. Modelling the out-of-plane seismic behaviour of masonry walls by rigid elements. *Earthq Eng Struct Dyn* 2000;29(12):1797–813.
- [37] Roca P, Cervera M, Gariup G, Pela' L. Structural analysis of masonry historical constructions. Classical and advanced approaches. *Arch Comput Methods Eng* 2010;17:299–325.
- [38] Tralli A, Alessandri C, Milani G. Computational methods for masonry vaults: a review of recent results. *Open Civil Eng J* 2014;8(8):272–87.
- [39] Ferreira TM, Costa AA, Costa A. Analysis of the out-of-plane seismic behavior of unreinforced masonry: a literature review. *Int J Archit Herit* 2015;9(8):949–72.
- [40] Sorrentino L, D'Ayala D, de Felice G, Griffith MC, Lagomarsino S, Magenes G. Review of out-of-plane seismic assessment techniques applied to existing masonry buildings. *Int J Archit Herit* 2017;11(1):2–21.
- [41] D'Altri AM, Sarhosis V, Milani G, Rots J, Cattari S, Lagomarsino S, et al. Modeling strategies for the computational analysis of unreinforced masonry structures: review and classification. *Arch Comput Methods Eng* 2020;27:1153–85.
- [42] Milani G, Lourenço PB, Tralli A. Homogenization approach for the limit analysis of out-of-plane loaded masonry walls. *J Struct Eng* 2006;132(10):1650–63.
- [43] Cecchi A, Milani G, Tralli A. A Reissner–Mindlin limit analysis model for out-of-plane loaded running bond masonry walls. *Int J Solids Struct* 2007;44(5):1438–60.
- [44] Chen Z, Zhou Y, Kinoshita T, DeJong MJ. Distinct element modeling of the in-plane and out-of-plane response of ordinary and innovative masonry infill walls. *Structures* 2023;50:1447–60.

- [45] Kesavan P, Menon A. Investigation of in-plane and out-of-plane interaction in unreinforced masonry piers by block-based micro-modeling. *Structures* 2022;46:1327–44.
- [46] Chan HSY. The collapse load of reinforced concrete plate. *Int J Numer Methods Eng* 1972;5(1):57–64.
- [47] Munro J, Da Fonseca AMA. Yield-line method by finite elements and linear programming. *Struct Eng* 1978;56(12):37–44.
- [48] Chiozzi A, Milani G, Grillanda N, Tralli A. A fast and general upper-bound limit analysis approach for out-of-plane loaded masonry walls. *Meccanica* 2018;53:1875–98.
- [49] Gilbert M, Smith CC. Discontinuity layout optimization: a new numerical procedure for upper bound limit analysis. In: IX international conference on computational plasticity; 2007. p. 170–3.
- [50] Valentino J, Gilbert M, Gueguin M, Smith CC. Limit analysis of masonry walls using discontinuity layout optimization and homogenization. *Int J Numer Methods Eng* 2023;124(2):358–81.
- [51] He L, Gilbert M, Shepherd M. Automatic yield-line analysis of practical slab configurations via discontinuity layout optimization. *J Struct Eng* 2017;143(7):04017036.
- [52] Hawksbee S, Smith C, Gilbert M. Application of discontinuity layout optimization to three-dimensional plasticity problems. *Proc R Soc A, Math Phys Eng Sci* 2013;469(2155):20130009.
- [53] LimitState Ltd. LimitState:SLAB manual (version 2.3.1). Sheffield, UK: LimitState Ltd; 2021.
- [54] Orduña A, Lourenço PB. Three-dimensional limit analysis of rigid blocks assemblages. Part I: torsion failure on frictional interfaces and limit analysis formulation. *Int J Solids Struct* 2005;42(18–19):5140–60.
- [55] Casapulla C, Mousavian E, Argiento L, Ceraldi C, Bagi K. Torsion-shear behaviour at the interfaces of rigid interlocking blocks in masonry assemblages: experimental investigation and analytical approaches. *Mater Struct* 2021;54(3):134.
- [56] Mojsilović N. Masonry elements with damp-proof course membrane: assessment of shear strength parameters. *Constr Build Mater* 2012;35:1002–12.
- [57] Braestrup M. Yield-line theory and limit analysis of plates and slabs. *Mag Concr Res* 1970;22(71):99–106.
- [58] Timoshenko S, Goodier JN. *Theory of elasticity*. 2 ed. McGraw-Hill Book Company; 1951.
- [59] He L, Grillanda N, Valentino J, Gilbert M, Smith C. Analysis of masonry arch bridges using multi-scale discontinuity layout optimization. In: *Life-cycle of structures and infrastructure systems*. CRC Press; 2023. p. 1376–83.
- [60] Marti P, Kong K. Response of reinforced concrete slab elements to torsion. *J Struct Eng* 1987;113(5):976–93.
- [61] Shin M, Bommer A, Deaton JB, Alemdar B. Twisting moments in two-way slabs. *Concr Int* 2009;31(7):35–40.
- [62] MATLAB. Version 9.12.0 (R2022a). Natick, Massachusetts: The MathWorks Inc.; 2022.
- [63] Southcombe C, May IM, Chong VL. The behaviour of brickwork panels with openings under lateral load. In: *Proceedings of the British masonry society*, vol. 7; 1995. p. 105–10.
- [64] Casolo S, Milani G. A simplified homogenization-discrete element model for the non-linear static analysis of masonry walls out-of-plane loaded. *Eng Struct* 2010;32(8):2352–66.
- [65] Silva LC, Lourenço PB, Milani G. Nonlinear discrete homogenized model for out-of-plane loaded masonry walls. *J Struct Eng* 2017;143(9):04017099.
- [66] Pantò B, Cannizzaro F, Calì I, Lourenço PB. Numerical and experimental validation of a 3D macro-model for the in-plane and out-of-plane behavior of unreinforced masonry walls. *Int J Archit Herit* 2017;11(7):946–64.
- [67] Silva LC, Lourenço PB, Milani G. Derivation of the out-of-plane behaviour of masonry through homogenization strategies: micro-scale level. *Comput Struct* 2018;209:30–43.
- [68] Bui T-T, Limam A, Sarhosis V. Failure analysis of masonry wall panels subjected to in-plane and out-of-plane loading using the discrete element method. *Eur J Environ Civ Eng* 2021;25(5):876–92.